

Spatiotemporal variation of late Quaternary river incision rates in southeast Tibet, constrained by dating fluvial terraces

Jin-Yu Zhang^{1,*}, Jing Liu-Zeng¹, Dirk Scherler^{2,3}, An Yin⁴, Wei Wang¹, Mao-Yun Tang¹, and Zhan-Fei Li¹

¹STATE KEY LABORATORY OF EARTHQUAKE DYNAMICS, INSTITUTE OF GEOLOGY, CHINA EARTHQUAKE ADMINISTRATION, BEIJING 100029, CHINA

²GFZ GERMAN RESEARCH CENTRE FOR GEOSCIENCES, 14473 POTSDAM, GERMANY

³INSTITUTE OF GEOLOGICAL SCIENCES, FREIE UNIVERSITÄT BERLIN, 12249 BERLIN, GERMANY

⁴DEPARTMENT OF EARTH, PLANETARY, AND SPACE SCIENCES, UNIVERSITY OF CALIFORNIA, LOS ANGELES, CALIFORNIA 90095-1567, USA

ABSTRACT

River incision results from interactions among tectonics, climate change, and surface processes, and yet the role of each process operating at different time scales remains poorly understood. In this study, we address this issue by reconstructing the late Quaternary spatiotemporal variation of aggradation and incision rates along the Lancang River (Upper Mekong River) in southeast Tibet. Our work combined field observations, topographic data analysis, and optically stimulated luminescence (OSL) and cosmogenic radionuclide (CRN) dating of geologically well-defined fluvial terrace deposits, and it reveals five levels of fluvial terraces with strath heights up to 200–240 m and a 300-km-wide knickzone along the Lancang River. The new data indicate that: (1) the Lancang River has experienced four aggradation events at >120–100 ka, 90–70 ka, 25–15 ka, and <9 ka, with each event followed by rapid incision at ca. 100 ka, ca. 45 ka, ca. 15 ka, and ca. 6 ka; (2) river incision rates since the late Pleistocene decrease upstream across the knickzone from <2.8–2.3 and <2.1–1.7 to <0.5 mm/yr; and (3) they decrease with time at the knickzone from <2.1 mm/yr at ca. 100 ka to <1.1 mm/yr at 15–6 ka. The terrace-derived incision rates since the late Pleistocene from this study are more than an order of magnitude higher than the existing landscape-scale erosion rates derived from both thermochronological dating of bedrock bounding the river valley at million-year scales and cosmogenic nuclide concentrations of river sand at millennial scales. These findings imply decoupling of hydrologically induced river incision rates since the late Pleistocene from regional erosion rates on million-year and millennial time scales. Specifically, the hydrologically driven incision in a large fluvial system like the Lancang River in southeast Tibet, most likely related to local climate conditions, is much more efficient than tectonically driven erosion at a time scale of 100–10 k.y.

LITHOSPHERE, v. 10; no. 5; p. 662–676 | Published online 4 September 2018

<https://doi.org/10.1130/L686.1>

INTRODUCTION

The closely spaced (~50 km apart) and parallel segments (~200 km long) of the Nu-Salween, Lancang-Mekong, and Jinsha-Yangtze Rivers are the most dominant drainage systems in southeast Tibet (Fig. 1; Brookfield, 1998; Hallet and Molnar, 2001; Clark et al., 2006). These rivers carved up to 3000-m-deep valleys that are bounded by regions displaying relics of low-relief surfaces on top of the valley-bounding ranges (Clark et al., 2006; Liu-Zeng et al., 2008). The geometry of the drainage basins is characterized by an abnormally low width-length ratio of ~0.0074 (Gregory and Gregory, 1925; Hallet and Molnar, 2001). These first-order observations have been used to infer plateau-uplift mechanisms (e.g., Clark et al., 2006), surface processes during plateau construction (e.g., Liu-Zeng et al., 2008; Yang et al., 2015), and tectonic strain (e.g., Brookfield, 1998; Hallet and Molnar, 2001; Clark et al., 2006) and lower-crustal flow (Clark et al., 2004) during the Indo-Asian collision.

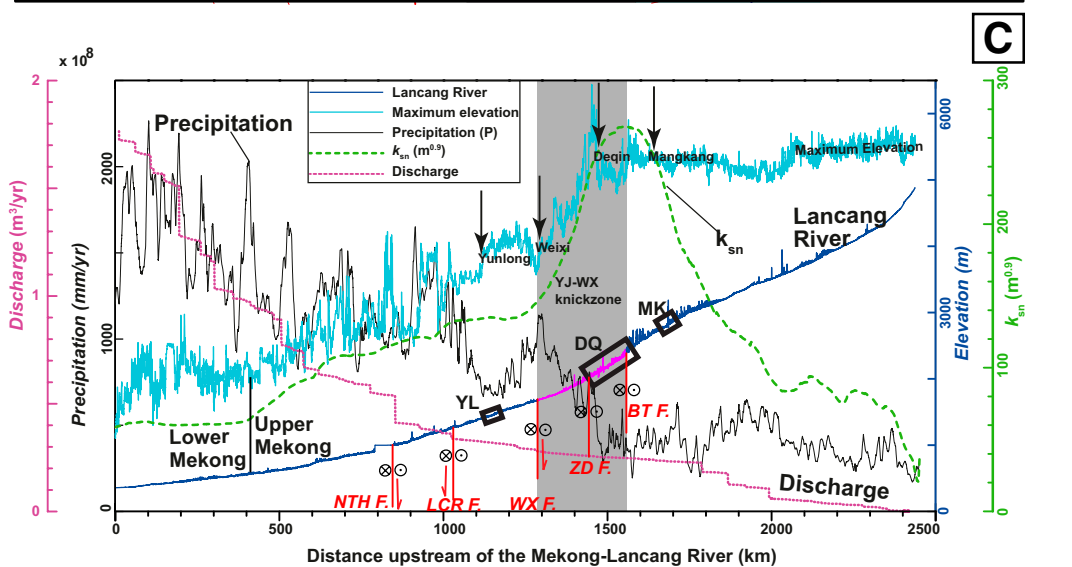
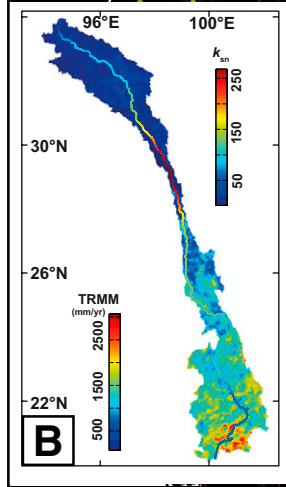
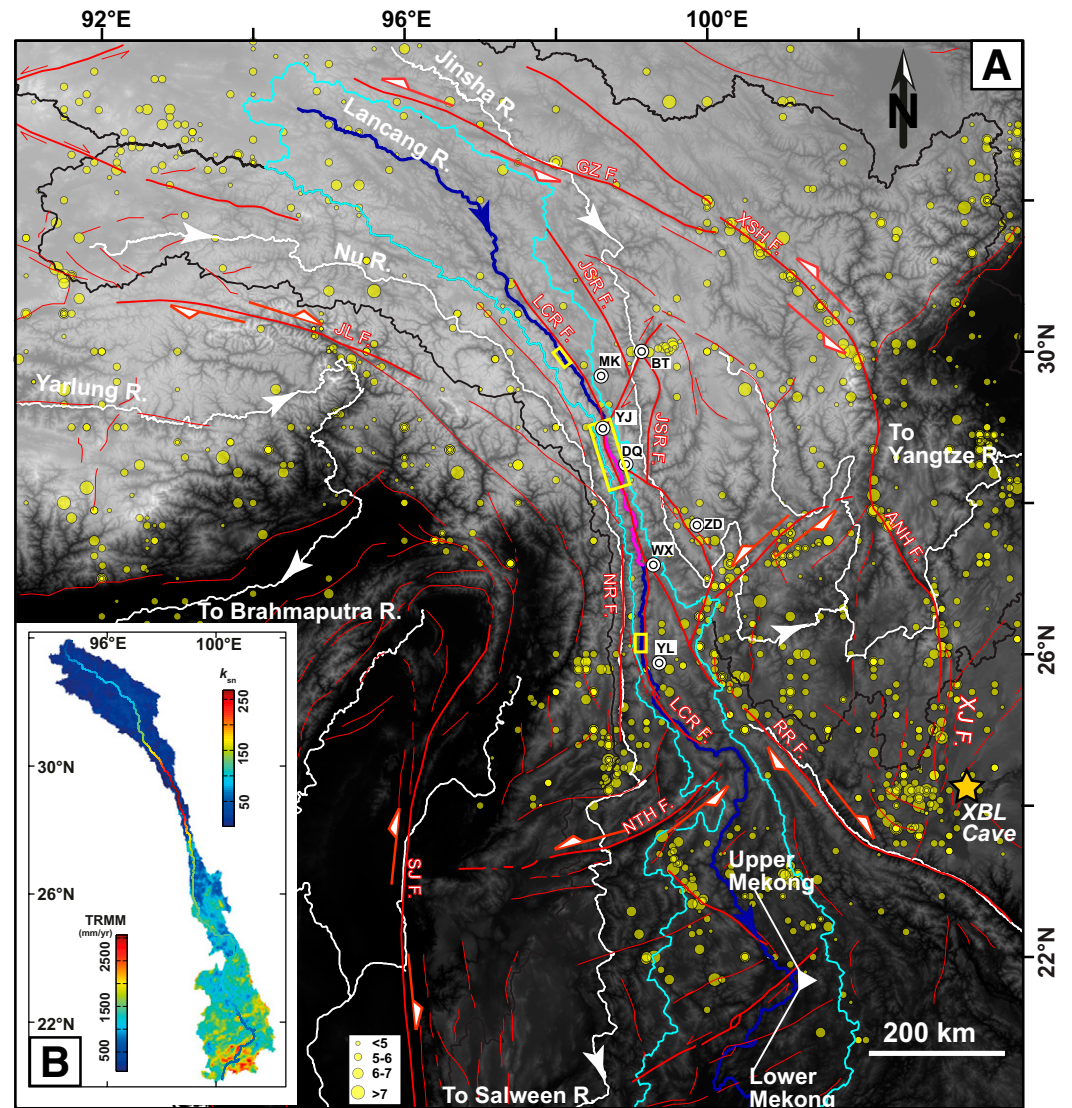
Although stimulating, these existing studies are mostly conceptual or based on inferences from numerical modeling. As a result, the roles of

different competing processes operating at different time scales during the landscape evolution of a tectonically active region remain poorly quantified. Even when high-quality river incision data are locally available in southeast Tibet, they typically represent an averaged effect over either a specific duration of geologic time or a defined space. For example, low-temperature thermochronometry has been used to quantify the bedrock exhumation rates over million-year time scales (Clark et al., 2005; Schoenbohm et al., 2006; Ouimet et al., 2010; Tian et al., 2014; Zhang et al., 2015; H.P. Zhang et al., 2016; Yang et al., 2016; Liu-Zeng et al., 2018), whereas in situ-produced cosmogenic ¹⁰Be concentrations of modern river sand provide basin-averaged denudation rates at a millennial time scale over the recent several thousand years (e.g., Henck et al., 2011). Although these approaches have provided important constraints on landscape evolution in southeast Tibet, there are very few direct measurements of incision rates using dated fluvial terraces in a single drainage basin from a river that cuts across the southeastern margin of Tibet.

In this study, we combined field observations, digital topographic analysis, and optical stimulated luminescence (OSL) and cosmogenic radionuclide (CRN) dating of multiple levels of fluvial terraces preserved along the Lancang River to quantify the late Quaternary spatial and temporal

*Corresponding Author: jinyuzhang87@foxmail.com

Figure 1. (A) Topographic map of southeast Tibet based on 90-m-resolution Shuttle Radar Topography Mission (SRTM) digital elevation model, showing the distribution of major river systems, active faults, and historical earthquakes. The main rivers, i.e., Yarlung-Brahmaputra, Nu-Salween, and Jinsha-Yangtze Rivers, are marked by white lines, whereas the Lancang-Mekong River in this study is marked by blue lines, with the Yanjing-Weixi knickzone between Yanjing (YJ) and Weixi (WX) highlighted by the purple line. Yellow rectangles show three study reaches with fluvial terraces along the Lancang River, near Mangkang (MK), Deqin (DQ), and Yunlong (YL). Active faults are marked by red lines with arrows to indicate direction of horizontal motion of main strike-slip faults, based on the work by Tapponnier et al. (2001), Deng et al. (2003), and Taylor and Yin (2009). ANH F.—Anninghe fault; JL F.—Jiali fault; GZ F.—Ganzi fault; XSH F.—Xianshuihe fault; XJ F.—Xiaojiang fault; RR F.—Red River fault; JSR F.—Jinsha River fault; LCR F.—Lancang River fault; NR F.—Nu River fault; NTH F.—Nantinghe fault; SJF—Shijie fault. Historical earthquakes from 780 B.C. to 2008 are cited from China Earthquake Networks Center (<http://www.ceic.ac.cn/history>). Geographic names include: BT—Batang; ZD—Zhongdian; and WX—Weixi. Yellow star marks the location of the Xiaobailong Cave in southeast Tibet (XBL; Cai et al., 2015). (B) Spatial distribution of annually averaged precipitation across the Lancang drainage basin derived from Tropical Rainfall Measuring Mission (TRMM) data (adapted from <http://www.geog.ucsb.edu/~bodo/TRMM/>) and normalized (reference concavity $\theta_{ref} = 0.45$) steepness indices, k_{sn} , along the Lancang River determined by the integral method (Perron and Royden, 2013; Mudd et al., 2014). (C) Longitudinal profile for the Lancang River (blue) and its drainage divide (cyan), TRMM-derived precipitation (black), normalized channel steepness (green), and river discharge with drainage area weighted by TRMM data (purple). Black arrows point to geographic locations within the Lancang drainage area as shown in part A. The Yanjing-Weixi knickzone is highlighted in purple with gray background, while the three reaches with fluvial terraces in this study are denoted by black rectangles. Right-lateral active faults intersecting with the Lancang River channel are also indicated as follows: BT F.—Batang fault; ZD F.—Zhongdian fault; WX F.—Weixi fault; and LCR F.—Lancang River fault; NTH F.—Nantinghe fault.



variation of river incision rates in southeast Tibet. These terraces provide average incision rates of the main trunk valley of the Lancang River at time scales of 100–10 k.y. They thus fill the time gap between the million-year time scale obtained by the thermochronological methods and the recent millennial time scale estimated from ^{10}Be concentrations in stream sediments. Furthermore, the distribution of fluvial terraces and their spatial variation in height above the river provide important information on the spatiotemporal patterns of river incision, which may help to discern between tectonic and climate processes controlling river incision (e.g., Burbank et al., 1996; Whipple, 2004; Whittaker, 2012).

The most important findings of this work include: (1) the average river incision rate since the late Pleistocene is more than an order of magnitude higher than the averaged erosion rates over million-year and millennial time scales as derived from thermochronological and cosmogenic ^{10}Be concentrations methods, (2) the river incision rates since the late Pleistocene decrease upstream, and (3) the river incision rates within the knickzone decrease with time from the late Pleistocene to Holocene. These results suggest that the spatial pattern of climate conditions and hydrologic response with time may play an important role in modulating river incision rates at various space and time scales in a tectonically active region.

REGIONAL GEOLOGIC AND CLIMATIC SETTINGS

The >2000-km-long Lancang River descends ~4000 m in elevation from southeast Tibet to the lower segment of the Mekong River that enters the South China Sea (Fig. 1). Near Deqin (Fig. 1C), the regional topography transitions from a low-relief region in the northwest to a more rugged region farther southeast, and the average elevation decreases from >5000 m to ~2000 m over a distance of ~1000 km. Within this transition zone, the longitudinal profile of the Lancang River exhibits an ~300-km-long knickzone between Yanjing and Weixi, hereafter referred to the Yanjing-Weixi knickzone (Fig. 1C). Across the knickzone, the river decreases in elevation downstream from ~2400 m to ~1700 m, whereas the normalized (reference concavity $\theta_{\text{ref}} = 0.45$) channel steepness indices (k_{sn}), determined by the integral method (Perron and Royden, 2013; Mudd et al., 2014), decrease from 270 to 140 $\text{m}^{0.9}$ (Figs. 1B and 1C).

The Lancang drainage basin is situated in the Qiangtang terrane in the north and the Lanping-Simao terrane in the south (Pan et al., 2004; Burchfiel and Chen, 2012). Above the Yanjing-Weixi knickzone, the Lancang River mainly flows across Mesozoic sedimentary rocks of the Qiangtang terrane, especially the Middle Triassic strata containing felsic and intermediate volcanic rocks at latitudes of 30°N–29°N. At the knickzone, the river flows dominantly within Paleozoic sedimentary rocks of the Qiangtang terrane. Downstream from the knickzone, the river flows across Mesozoic sedimentary rocks, including Late Triassic mafic volcanic rocks of the Lanping-Simao terrane. South of Yunlong, the river cuts across the Chongshan mylonitic shear zone.

The Lancang drainage basin is cut by the active right-lateral Jinsha River, Red River, and Lancang River fault zones, and a left-lateral fault system near 24°N (Fig. 1A; Tapponnier et al., 2001; Deng et al., 2003; Taylor and Yin, 2009). The Lancang River fault zone trends mostly sub-parallel to the main trunk of the Lancang River between 25°N and 31°N, but it cuts across the river at several locations. South of Yunlong (Fig. 1A), where the Lancang River fault zone intersects the Lancang River, the hairpin-shaped river-trunk geometry and the displaced tributaries on the east side of the river indicate right-lateral strike-slip motion with a west-side-down normal-fault component. The NNE-striking Batang fault, the NW-striking Zhongdian fault, the NW-striking Weixi fault, and the NWW-striking Nantinghe fault intersect the Lancang River obliquely,

with the latter two structures dipping to the north (Figs. 1A and 1C). The Yanjing-Weixi knickzone along the Lancang River is situated between the right-lateral Batang and Weixi faults (Figs. 1A and 1C). Thus, the formation of the knickzone may have been related to transpression due to motion along the two faults. Alternatively, the knickzone may have been generated by differential vertical motion across the Lancang River fault zone.

Two climate systems dominate our study area at present: the mid-latitude westerlies and the Indian monsoon. In this region, the wet summer monsoon season lasts for 4 months from June to September, and the resultant discharge transports 86% of the suspended sediment load (Henck et al., 2010). Subparallel ridges and valleys in southeast Tibet exert a strong topographic control on the spatial distribution of precipitation. The north-trending valleys act as conduits to transmit moisture upstream, whereas the intervening ridges act as barriers that block transport of moisture eastward. Along the Lancang River, mean annual precipitation derived from Tropical Rainfall Measuring Mission (TRMM) data decreases upstream from 2000 to 340 mm/yr, with a sharp drop near the plateau topographic transition zone near Deqin (Fig. 1). The Lancang drainage basin also encompasses the southeastern edge of active glacial areas in southeast Tibet.

METHODS

Fluvial terraces perched above the active channel of the Lancang River were first mapped using Google Earth™ images. In the field, we measured the heights of terrace treads and bedrock straths using a laser rangefinder and established the terrace stratigraphy and its lateral correlative relationships. This field-based geological framework allowed us to collect meaningful OSL and CRN samples, with which we determined the timing of key geologic events related to river evolution.

OSL Dating

We obtained burial ages of terrace sediments using the quartz OSL method. Samples were collected from fine-grained sand to silt lenses embedded in terrace deposits as close to the bedrock surfaces as possible. By doing so, the obtained dates offer a minimum age of strath-surface formation. Both the accuracy and precision of OSL dating depend on how completely quartz grains are bleached prior to deposition, which is controlled by the intensity and duration of exposure to daylight during sediment transport (e.g., Rhodes, 2011). The origin and geologic history of the quartz grains are also important: Grains recently eroded from bedrock are much more difficult to bleach than those that have experienced multiple cycles of deposition and reworking at the surface (Rhodes, 2011; J.Y. Zhang et al., 2016). Considering the fluvial origin of the samples along the mostly turbulent Lancang River, we expect the possibility of partially bleached grains, which would result in an overestimation of depositional ages of terrace sediments (i.e., the actual ages of terrace sedimentation could be younger; Rodnight et al., 2006).

All OSL samples were collected in stainless-steel tubes with ~5 cm inner diameter and ~25 cm length. After sampling, both ends of the tubes were immediately sealed with aluminum foil and wrapped with opaque tape to limit exposure to sunlight. In addition, the ~5 cm outer sediments near the ends of the tube were removed in the laboratory before mineral separation. The samples were prepared to extract purified quartz following conventional techniques (Aitken, 1998). OSL age determination was performed at the Luminescence Dating Laboratory of the Institute of Geology, China Earthquake Administration. The sensitivity-corrected multiple-aliquot regenerative-dose protocol (SMAR) was applied for most of our samples to yield one value of equivalent dose (D_e) for each sample

(Wang et al., 2005; Lu et al., 2007). This protocol uses multiple aliquots of fine-grained quartz grains (4–11 μm) to build the growth curve, and it corrects the sensitivity changes with a test dose to each aliquot. Compared with the single-aliquot regenerative-dose protocol (SAR), the advantage of this protocol lies in avoiding high levels of OSL recuperation for samples with De >120 Gy (up to 8%) and the resultant age underestimation (Wang et al., 2005; Lu et al., 2007). However, this protocol does not allow the degree of bleaching to be evaluated with multiple De values by either radial plots or probability histograms (Thrasher et al., 2009; Rhodes, 2011). For equivalent dose <120 Gy, the SAR protocol was further applied to coarser-grained quartz grains of 90–125 μm size to identify grains that were completely bleached and that would yield a more reliable OSL age (Murray and Wintle, 2003).

Cosmogenic Nuclide (¹⁰Be) Dating

In situ-produced cosmogenic ¹⁰Be in quartz dates the exposure ages of terrace surfaces to cosmic rays (e.g., Lal, 1991; Gosse and Phillips, 2001; Dunai, 2010). These exposure ages are typically interpreted to indicate the time when rivers incised and abandoned a terrace tread (e.g., Anderson et al., 1996; Repka et al., 1997; von Blanckenburg and Willenbring, 2014). However, individual clasts exposed on terrace treads likely experienced a protracted history of exhumation, transport, and transient burial and are therefore likely to start with different nuclide concentrations at the time of exposure. We amalgamated at least 30 individual pebbles of 1–3 cm size to average the inheritance of cosmogenic nuclides and obtain an upper limit for the time of terrace abandonment (Repka et al., 1997). To avoid local sources, we collected rounded pebbles, indicative of substantial transport distance, far from adjoining

hillslopes. In addition, we amalgamated 3–5-cm-thick rock chips from the top of five to seven large (i.e., >1 m wide and tall) and presumably stable boulders that were imbedded within the terrace tread. As boulders of this size likely originate from landslides, they probably have only very little inheritance in ¹⁰Be concentrations. Furthermore, postdepositional erosion of the boulders tends to make the exposure ages younger, and we would expect that the amalgamated boulder samples would be younger than the amalgamated pebble samples. Both kinds of samples were collected from areas as flat as possible, without any apparent anthropogenic modification and away from the edges of the terrace surfaces to minimize postdepositional erosion.

Separation and purification of quartz grains and chemical extraction of beryllium were done following the revised method of von Blanckenburg et al. (2004) at the Helmholtz Laboratory for the Geochemistry of the Earth Surface (HELGES) at the GFZ German Research Center for Geosciences. Subsequent isotope measurements for cosmogenic ¹⁰Be were conducted at the accelerator mass spectrometer facility at the University of Cologne in Germany (Dewald et al., 2013). Table 1B lists the analytical sample results and the associated 1σ uncertainties, based on the propagated uncertainties in the carrier concentration, one process blank, and the isotope measurements. We calculated exposure ages from ¹⁰Be concentrations using the CRONUS-Earth online calculator v. 2.3 (Balco et al., 2008). The exposure ages reported here are based on the time-dependent version of the Lal (1991)/Stone (2000) production scaling model (“Lm” in Balco et al., 2008). Our samples were collected from high-relief valleys, and we thus corrected for topographic shielding using 90-m-resolution Shuttle Radar Topography Mission (SRTM) data and following Dunne et al. (1999). Shielding by snow or vegetation is negligible for the CRN samples collected in our study.

TABLE 1A. OPTICALLY STIMULATED LUMINESCENCE (OSL) DATING RESULTS FOR TERRACE DEPOSITS ALONG THREE REACHES OF THE LANCANG RIVER

Sample no.	Lab code	Latitude (°N)	Longitude (°E)	Elevation (m)	Burial depth (m)	Method	U-238 (Bg/kg)	Ra-226 (Bg/kg)	Th-232 (Bg/kg)	K-40 (Bg/kg)	Water content (%)	Dose rate (Gy/k.y.)	De (Gy)	Age ± (ka)
Mangkang reach														
MK14-01	LEDL15-73	29.96517	98.06708	2929	1	SMAR	36.0 ± 4.2	39.2 ± 0.4	56.7 ± 0.5	772.6 ± 12.3	3	4.3 ± 0.3	259.0 ± 20.0	59.9 4.9
MK14-02	LEDL14-388	29.96882	98.06416	2923	1.5	SMAR	32.7 ± 3.7	31.4 ± 0.3	47.1 ± 0.5	615.3 ± 9.9	2	3.5 ± 0.4	305.8 ± 19.8	88.7 6.2
Deqin reach														
YJ15-01	LEDL16-216	29.021614	98.604222	2425	5	SMAR	28.3 ± 5.9	25.8 ± 0.4	42.4 ± 0.5	580.8 ± 9.9	1	3.1 ± 0.3	274.8 ± 17.1	89.1 6.0
YJ15-02	LEDL16-217	28.980767	98.631133	2465	5	SMAR	24.5 ± 5.3	22.9 ± 0.4	33.5 ± 0.4	385.6 ± 7.1	0	2.4 ± 0.2	236.6 ± 34.2	100.2 14.7
DQ14-02	LEDL15-71	28.45559	98.830684	2201	13.2	SMAR	31.8 ± 4.0	33.1 ± 0.4	57.6 ± 0.5	620.9 ± 10.1	9	3.3 ± 0.3	295.4 ± 19.3	89.1 6.3
XD15-01	LEDL16-211	28.452525	98.834383	2082	1.2	SMAR	32.7 ± 5.4	26.7 ± 0.4	34.1 ± 0.4	437.1 ± 7.7	1	2.7 ± 0.2	42.5 ± 1.7	15.6 0.7
DQ14-03	LEDL14-390	28.371722	98.863389	2029	9.8	SAR	29.1 ± 6.1	27.3 ± 4.8	39.5 ± 0.6	504.4 ± 8.3	7	2.3 ± 0.2	20.3 ± 0.4	9.0 0.3
YL15-01	LEDL16-215	28.298264	98.865439	2167	2.5	SMAR	38.3 ± 5.8	23.4 ± 0.4	35.7 ± 0.4	441.8 ± 8.0	0	2.7 ± 0.2	316.0 ± 34.2	116.6 13.0
DQ14-05	LEDL15-72	28.283333	98.8625	2059	2	SMAR	31.9 ± 3.7	32.5 ± 0.4	45.5 ± 0.4	579.8 ± 9.4	3	3.3 ± 0.3	280.6 ± 14.6	86.0 5.0
DQ14-04	LEDL14-391	28.290972	98.859972	2048	11.6	SAR	36.1 ± 3.6	34.5 ± 0.4	50.4 ± 0.5	641.9 ± 10.2	6	2.9 ± 0.2	112.4 ± 8.4	38.6 3.0
Yunlong reach														
TE15-07	LEDL16-213	26.164797	99.126038	1728	3	SMAR	37.5 ± 6.3	35.8 ± 0.5	46.6 ± 0.5	628.0 ± 10.6	3	3.5 ± 0.3	355.1 ± 15.3	100.4 5.1
TE15-08	LEDL16-214	26.16315	99.132186	1556	3	SMAR	37.4 ± 6.2	26.8 ± 0.5	43.9 ± 0.5	580.7 ± 10.0	0	3.3 ± 0.3	233.0 ± 21.3	71 6.7

Note: SMAR—sensitivity-corrected multiple-aliquot regenerative dose protocol for fine-grained quartz grains; SAR—single-aliquot regenerative dose protocol for fine-grained quartz grains; De—equivalent dose for the sample estimated in the laboratory.

TABLE 1B. COSMOGENIC RADIONUCLIDE (CRN) EXPOSURE DATING RESULTS FOR FLUVIAL TERRACES AT DEQIN REACH WITHIN THE YANJING-WEIXI KNICKZONE OF THE LANCANG RIVER

Sample no.	Latitude (°N)	Longitude (°E)	Elevation (m)	Location	Sample type	Shielding correction	¹⁰ Be concentration (atoms/g)	±	Exposure age (ka)	±
15-8-30-(1)	28.8079	98.6559	2335	Adong	Pebbles	0.940853	9.604E+05	3.131E+04	56.8	5.9
15-8-30-(2)	28.8079	98.6559	2335	Adong	Quartz vein	0.940853	8.032E+05	2.638E+04	46.1	4.7
15-6-2-(1)	28.4519	98.8293	2244	Xidang	Pebbles	0.977093	7.883E+05	2.593E+04	46.4	4.8
15-6-2-(5)	28.4487	98.8322	2102	Xidang	Pebbles	0.9572	2.339E+05	7.986E+03	17.1	1.7
15-6-3-(2)	28.3605	98.8672	2022	Junda	Boulder fragments	0.929468	7.335E+04	3.064E+03	5.96	6.1

River Incision Rates Derived from Fluvial Terraces

The strath surfaces of fluvial terraces along the Lancang River are overlain by alluvial deposits with a thickness 0.5–2 times the strath height above the current river. This indicates that river incision is far from a monotonous downcutting process, with possibly several successive episodes of strath abrasion, fill deposition, re-incision, and downcutting into the bedrock. Due to lateral migration associated with river aggradation or blockage events, a river channel may not systematically reoccupy an early course. Instead, it may erode the walls or shoulders of the former valley (Lavé and Avouac, 2001; Ouimet et al., 2007), and thus possibly create a strath surface that does not correspond to the bedrock floor of the former channel. Hence, the boundary between bedrock strath and its overlying alluvial deposits is likely to yield an upper limit on river incision into the bedrock. To minimize this uncertainty, we always measured the lowest strath exposed at a field site. Because of the unknown depth to the bedrock below the modern river surface and the thickness of the sediment cover, we used the modern river elevation as our reference level, which yields a minimum estimate for the amount of river incision. Compared with the ^{10}Be exposure dating of the topmost terrace deposits, which yields the time of incision (if erosion is zero), the OSL burial ages of the stratigraphically lowest alluvium directly above the strath surfaces should offer a lower age limit of the corresponding strath-carving event (Lavé and Avouac, 2001; Wegmann and Pazzaglia, 2009). In addition, most terrace deposits along the Lancang River in this study are thicker than the scour depth of the channel, which scales with the upstream drainage area (Pazzaglia, 2013), and we therefore interpret these sediments to have been deposited during some time period after strath cutting, which is difficult to evaluate more exactly (e.g., Lavé and Avouac, 2001; Scherler et al., 2014). With these limitations in mind, we calculated fluvial incision rates (I) along the river using $I = H_s/T_s$, where H_s is the elevation of strath surfaces (m), and T_s is the estimated age (ka) of strath formation (e.g., Lambeck et al., 2004; Wegmann and Pazzaglia, 2009). The uncertainty of the incision rate is $\sigma_I^2 = (\sigma_{H_s}/T_s)^2 + (H_s/T_s^2)^2\sigma_{T_s}^2$, where σ_{H_s} is the uncertainty in the height of strath surfaces (m) above the modern river, and σ_{T_s} is the OSL

uncertainty (ka). Table 2 summarizes the calculated incision rates together with the ages and heights of strath surfaces obtained in this study.

RESULTS

Fluvial Terraces

We studied fluvial terraces with strath surfaces that lie at 220–250 m, 140–170 m, 100–120 m, 35–60 m, and 10–20 m, respectively, above the Lancang River. The strath surfaces are overlain by alluvial deposits from 2 m to >100 m thick. In this study, we focused on the terraces located at Mangkang, Deqin, and Yunlong, which are above, at, and below the Yanjing-Weixi knickzone (Fig. 1).

Mangkang Reach

There are three levels of strath surfaces at the Mangkang reach at 220–240 m, 100–140 m, and 35–60 m above the present Lancang River (Figs. 2 and 3). A prominent subhorizontal terrace surface is 130–180 m above the river (Fig. 3B). The associated strath surface at 35–60 m is overlain by fluvial gravels, grading upward from boulders and cobbles at the base to pebbles and overbank deposits of silt and clay (Figs. 3C and 3D). Our two OSL ages from the top of the terrace deposits indicate that a river aggradation event occurred at >90–60 ka (Table 1A; Fig. 2A). In addition, a strath terrace is exposed at the height of ~220–240 m above the river, and it is capped by ~15-m-thick fluvial boulders, pebbles, and coarse- to medium-grained sand lenses (Fig. 3E).

Deqin Reach

We identified four levels of bedrock strath at 210–250 m, 140–190 m, 90–110 m, and 10–20 m along the Deqin reach, each capped by alluvial deposits (Figs. 2 and 4). A prominent strath surface at a height of 140–190 m above the river can be traced for ~80 km between Yanjing and Xidang along the main trunk (Figs. 4B–4E). The overlying terrace deposits consist of boulders, pebbles, and sand beds, locally overlain by colluvial and tributary fan deposits, and have thicknesses varying from

TABLE 2. SUMMARY OF OPTICALLY STIMULATED LUMINESCENCE (OSL) AND COSMOGENIC RADIONUCLIDE (CRN) DATING RESULTS FOR TERRACE DEPOSITS, HEIGHTS OF BEDROCK STRATH, AND RIVER INCISION RATES FOR FLUVIAL TERRACES ALONG THREE REACHES OF THE LANCANG RIVER

Location	Sample no.	Ages of terrace deposits (ka)		Height of strath (m)		River incision rate (mm/yr)		Dating method
Mangkang reach								
Mangkang	MK14-02	88.7	6.2	45	10	0.51	0.18	OSL
	MK14-01	59.9	4.9					OSL
Deqin reach								
Yanjing	YJ15-01	89.1	6	177	15	1.99	0.17	OSL
	YJ15-02	100.2	14.7	168	15	1.68	0.17	OSL
Adong	8-30-1	56.8	5.9	177	15			CRN
	8-30-2	46.1	4.7					CRN
Xidang	DQ14-02	89.1	6.3	155	15	1.74	0.17	OSL
	15-6-2-(1)	46.4	4.8					CRN
	XD15-01	15.6	0.7	16	2	1.03	0.14	OSL
	15-6-2-(5)	17.1	1.7					CRN
Junda	DQ14-03	9.0	0.3	10	1	1.11	0.12	OSL
	15-6-3-(2)	6.0	0.6					CRN
Yunling	YL15-01	116.6	13	243	20	2.08	0.18	OSL
	DQ14-05	86	5	104	10	1.21	0.13	OSL
	DQ14-04	38.6	3					OSL
Yunlong reach								
Yunlong	TE15-07	100.4	5.1	284	20	2.83	0.20	OSL
	TE15-08	71	6.7	166	15	2.34	0.22	OSL

Note: Bold indicates the selected ages of terrace deposits, height of strath, and river incision rates.

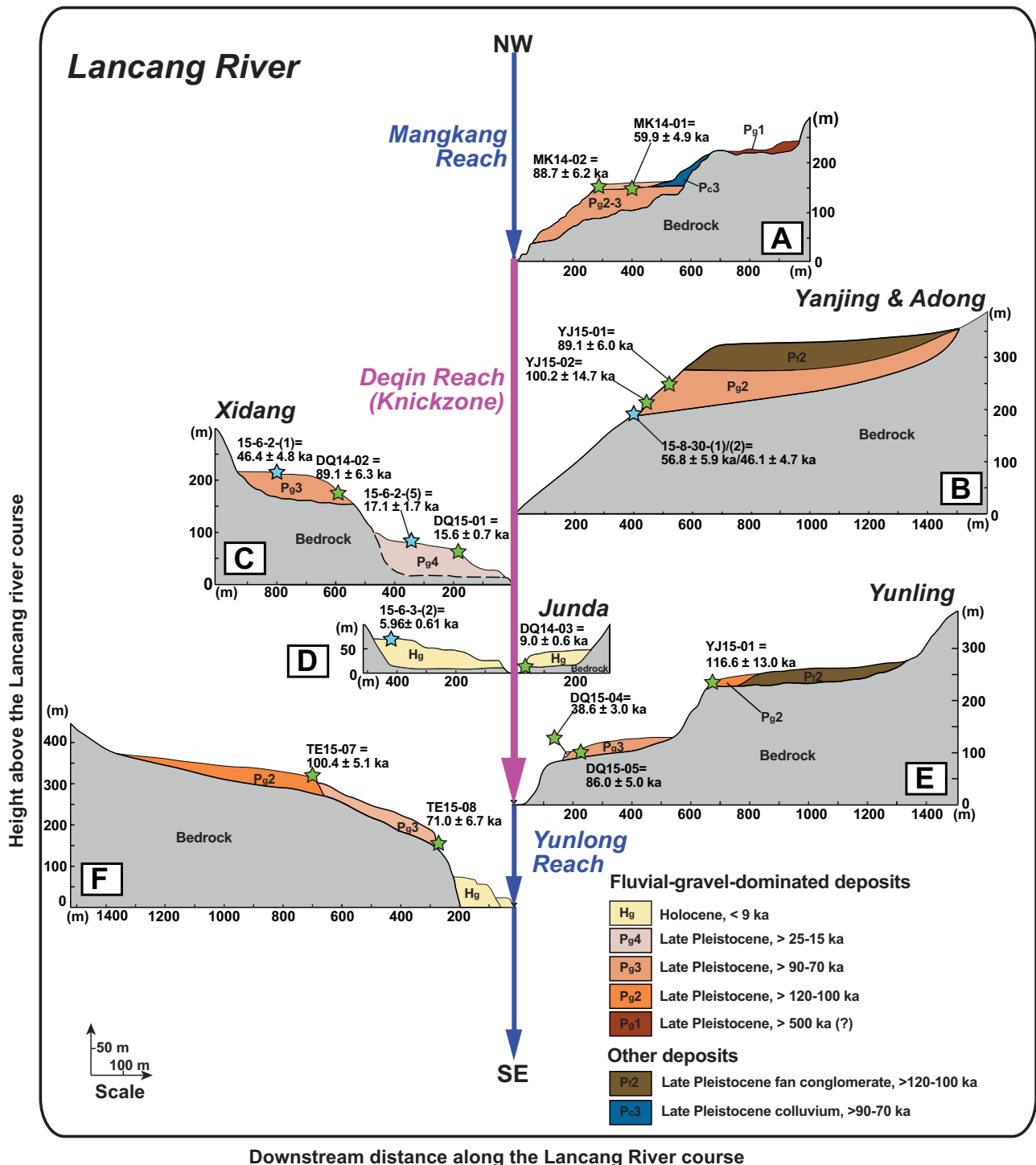


Figure 2. Simplified cross sections for various levels of fluvial terraces along the Lancang River: (A) Mangkang reach; (B–E) Deqin reach, including the Yanjing and Adong, Xidang, Junda, and Yunling sites; and (F) Yunlong reach. The locations and age results of optically stimulated luminescence (OSL) and cosmogenic radionuclide (CRN) samples are also shown by green and cyan stars, correspondingly.

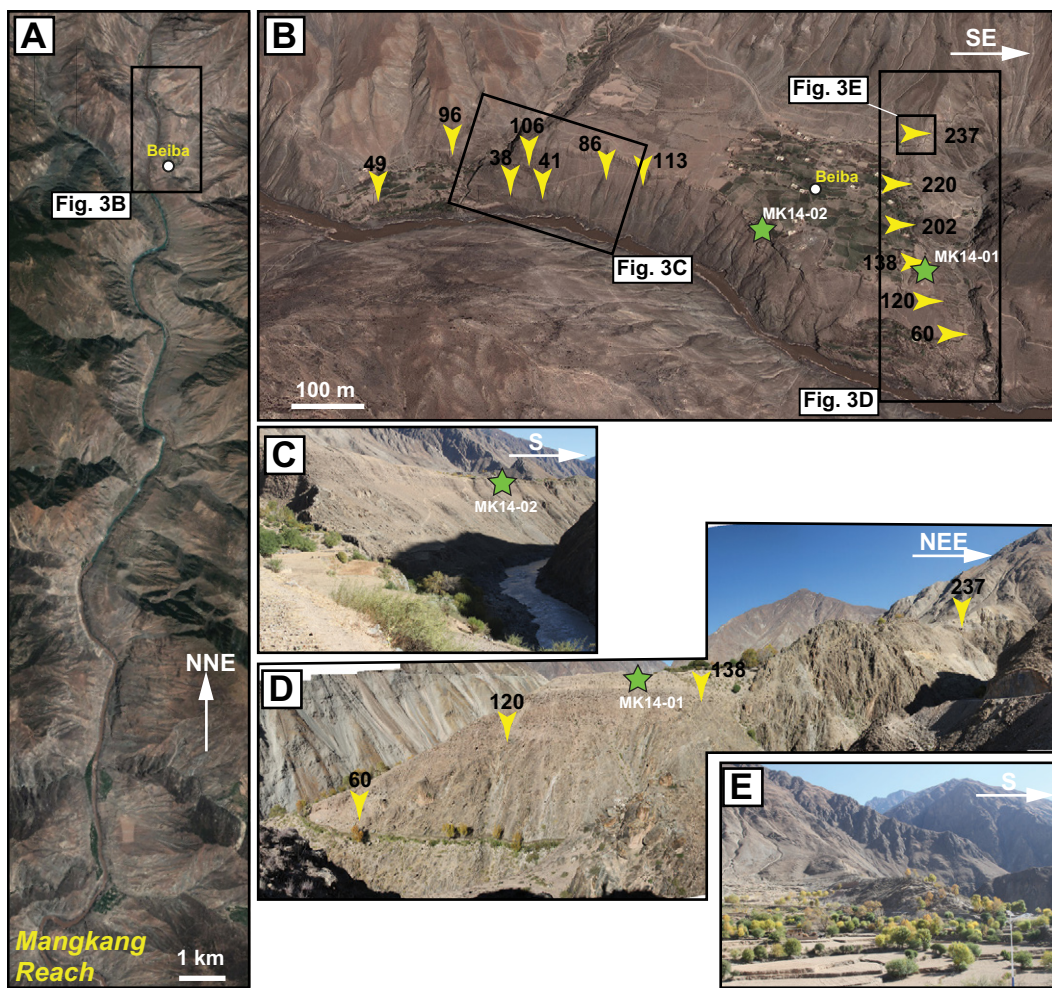


Figure 3. (A) Google Earth™ image showing the distribution of fluvial terraces for ~20 km along the Mangkang reach. Black rectangle shows the location of B. (B) Google Earth™ image at Beiba showing the prominent terrace tread at 130–180 m above the Lancang River, and bedrock straths at 100–140 m and 35–60 m, as marked by yellow arrow and black numbers. The locations of optically stimulated luminescence (OSL) samples MK14-01 and MK14-02 are marked by green stars. The locations of parts C, D, and E are denoted by black rectangles. (C) Field picture showing the prominent terrace tread at 130–180 m, where sample MK14-02 was collected, close to the Lancang River. (D) Field picture showing the vertical section of fluvial terrace to the south of Beiba with clear boundary between bedrock strath and its overlying terrace alluvium. (E) Field picture showing terrace deposits above bedrock strath at 220–240 m above the Lancang River.

10 m to 100 m. OSL dating of fine-grained sand layers close to the bedrock strath between Yanjing and Xidang revealed a regional aggradation event initiating before ca. 90 ka (Table 1A; Figs. 2B, 4C, and 4E). Three samples from terrace surfaces with bedrock straths at 140–190 m yielded CRN exposure ages of ca. 57–46 ka (Table 1B; Figs. 2B, 4D, and 4E), consistent with the OSL ages.

The highest terrace at Yunling has a bedrock strath at 210–250 m above the Lancang River that is capped by ~70-m-thick tributary fan conglomerates, and locally by fluvial gravels and thickly bedded fine-grained sand (Fig. 4F). OSL dating of a sand layer near the top of the terrace deposits indicates that this aggradation was under way at ca. 120 ka (Table 1A; Figs. 2D, 4F, and 4G). A lower strath surface lies at 90–110 m above the river, and it is overlain by 30–60-m-thick colluvium and tributary fluvial deposits. Two OSL ages from sand layers in the fluvial deposits reveal that aggradation started prior to 90 ka and ended no later than 40 ka (Table 1A; Figs. 2D and 4F). At Xidang, the lowest strath surface at 15–20 m is covered by a thick sequence of fluvial conglomerates, grading upward from boulders and cobbles to pebbles that are capped by overbank sand deposits (Fig. 4E). OSL dating of a sand layer near the terrace surface indicates that the transition from aggradation to incision occurred around 15 ka, compatible with CRN exposure dating of the terrace surface (Table 1; Figs. 2B and 4E). At Junda, the lowest strath surface lies at 8–10 m above the Lancang River, and it is capped

by 25-m-thick fluvial, boulder-to-cobble conglomerate with occasional sand lenses (Figs. 4H and 4I). The OSL age from a sand layer close to the bedrock strath indicates that river aggradation was under way at 9 ka, in agreement with a CRN exposure age of the terrace surface of 6 ka (Table 1; Figs. 2C, 4H, and 4I).

Yunlong Reach

The Yunlong reach below the Yanjing-Weixi knickzone features four levels of river terraces: two higher terraces with bedrock strath heights of 284 m and 150–170 m above the river, and two lower fill terraces with terrace surfaces at heights of 53 m and 21 m above the Lancang River (Figs. 2 and 5). At Songdeng, the 284 m strath is capped by boulder-to-cobble conglomerate and medium- to fine-grained sand and silt, whereas the 166 m strath is capped by well-rounded and well-sorted gravels of cobble to pebble size and medium- to fine-grained sand (Figs. 5B–5D). Both terrace treads and strath surfaces dip gently toward the Lancang River valley, indicating a high ratio of lateral planation to vertical incision during strath formation (e.g., Hancock and Anderson, 2002; Finnegan and Dietrich, 2011). OSL dating of sand deposits indicated that the corresponding aggradation events were under way at 100 ka and 70 ka (Table 1A; Figs. 2E, 5B, and 5D). Downstream at Songping, the bedrock strath is found at 158 m above the nearby river, overlain by reddish clay with angular gravels (Fig. 5E).

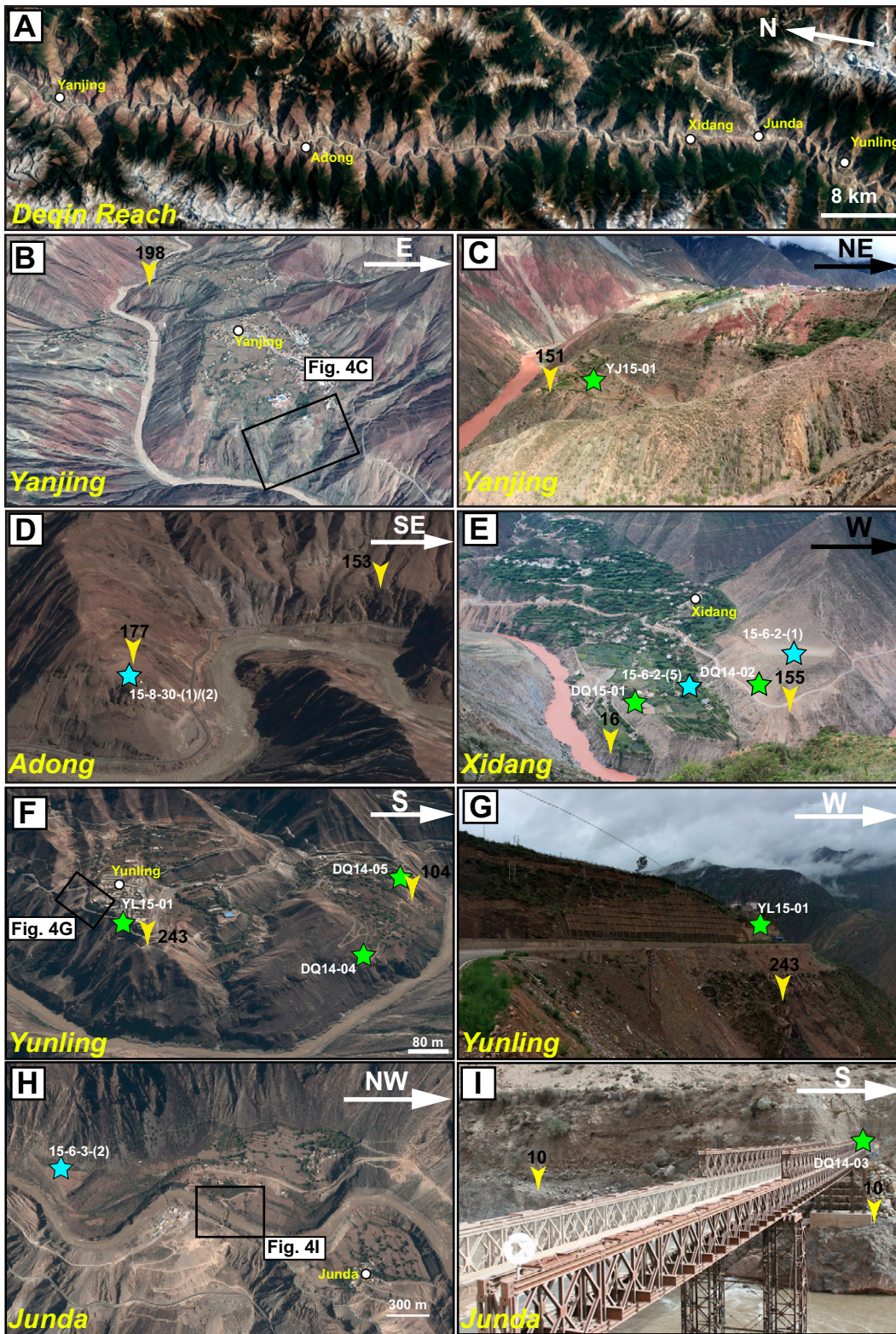


Figure 4. (A) Google Earth™ image showing the distribution of fluvial terraces along the Deqin reach. (B) Google Earth™ image at Yanjing showing the flat and extensive terrace tread at ~300 m above the Lancang River. Black boxes indicate the locations for part C. (C) Field picture showing the boundary between bedrock strath and overlying terrace alluvium at 151 m south of Yanjing. Terrace alluvium includes fluvial conglomerate and sand layers and the overlying colluvial deposits. Location of sample YJ15-01 is also shown. (D) Google Earth™ image east of Adong showing the bedrock platform at ~177 m, locally covered by 2-m-thick fluvial pebble gravels. Cosmogenic radionuclide (CRN) samples 15-8-30-1 and 15-8-30-2 are marked by cyan stars. (E) Field picture showing three levels of fluvial terraces at Xidang on the Deqin reach with two levels of bedrock straths at 155 m and 16 m. Green stars show locations of optically stimulated luminescence (OSL) samples DQ14-02 and DQ15-01, and cyan stars show locations for CRN samples 15-6-2-1 and 15-6-2-5. (F) Google Earth™ image for two levels of fluvial terraces at Yunling with bedrock straths at 243 and 104 m. Black box shows the location of part G, while green stars indicate locations of OSL samples YL15-01, DQ14-05, and DQ14-04. (G) Field picture of the eastern bank of the Lancang River at Yunling showing the boundary between bedrock strath and overlying terrace deposits at 243 m with OSL sample YL15-01 marked by green star. (H) Google Earth™ image showing three levels of fluvial terraces at Junda. Black boxes mark the location for field picture in part I, while cyan star marks the location of sample 15-6-3-2. (I) Field picture for the eastern bank of the Lancang River at Junda showing fluvial conglomerate interbedded with sand lens overlying 10 m bedrock strath with sample DQ14-03 marked by green star.

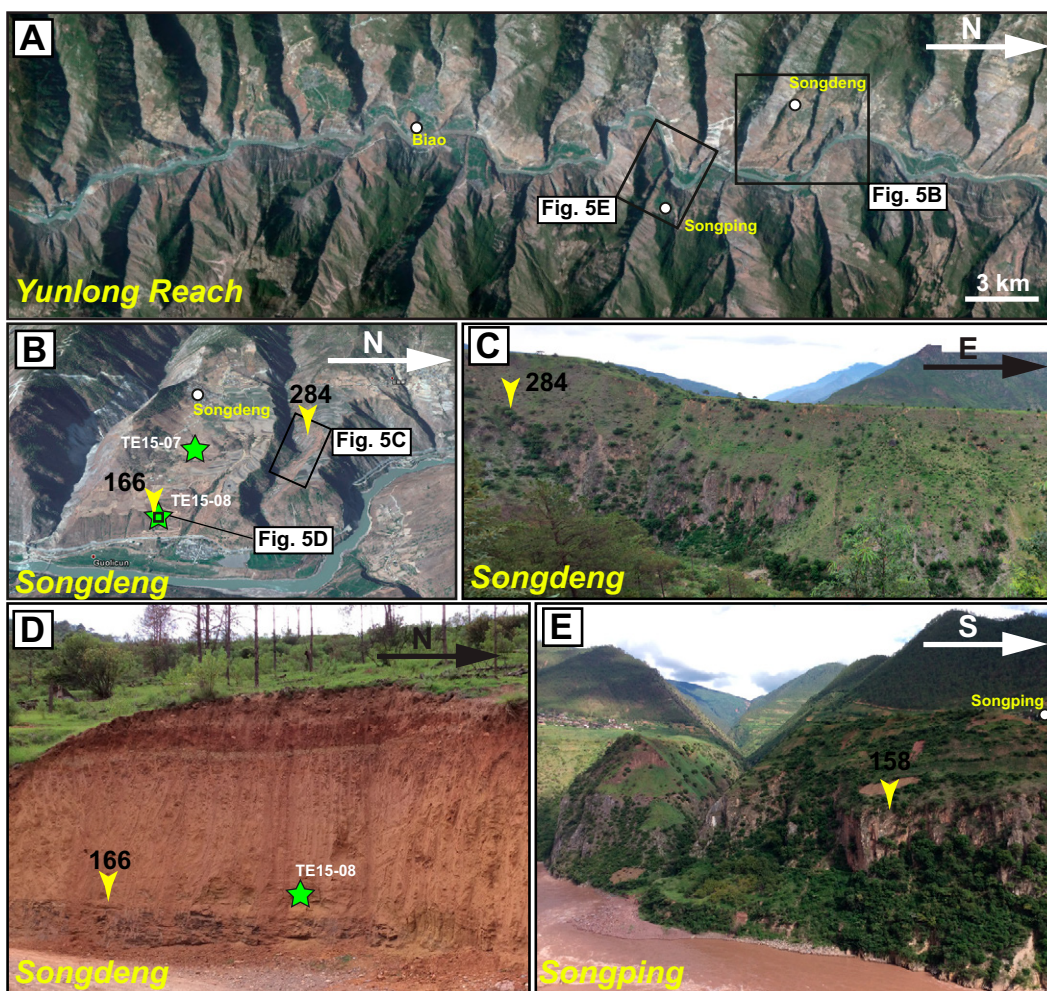


Figure 5. (A) Google Earth™ image showing the distribution of fluvial terraces along the Yunlong reach. Black boxes mark the locations of Songdeng and Songping in part B and E, correspondingly. (B) Google Earth™ image for the western bank of the Lancang River at Songdeng showing the gently dipping terrace with bedrock straths at 284 m and 166 m. Black boxes show the locations for field pictures in part C and D, and green stars indicate the locations of optically stimulated luminescence (OSL) samples TE15-07 and TE15-08. (C) Field picture north of Songdeng showing the boundary between terrace alluvium and bedrock strath at 284 m above the Lancang River. (D) Field picture to the east of Songdeng showing the strath-alluvium boundary at 166 m with OSL sample TE15-08 marked by green star. (E) Field picture showing the boundary between bedrock strath at 158 m with overlying terrace alluvium at Songping.

River Incision Rates

Our OSL and CRN exposure dating reveals four aggradation events at >120–100 ka, ca. 90–70 ka, ca. 25–15 ka, and <9 ka, each followed by incision that started no earlier than 100 ka, 45 ka, 15 ka, and 6 ka, respectively (Figs. 2 and 6). The incision rates related to each incision period are summarized in Table 2, and the procedures for obtaining them are described below.

Along the Mangkang reach, the river incision rate since <60 ka is <0.5 mm/yr (Fig. 6A). The highest strath level along the Deqin reach is 243 ± 20 m, and the upper limit of the incision rate since 100 ka is 2.1 mm/yr (Fig. 6D). The prominent bedrock strath at 140–190 m is overlain by terrace alluvium deposited at 90–70 ka, which yields an incision rate <1.7 mm/yr (Figs. 6B and 6C). The lower strath surface at 104 ± 10 m yields an upper limit for the incision rate prior to 40 ka of 1.2 mm/yr (Fig. 6D). For the lowest strath levels at 10–20 m above the river, the river incision rates since ca. 9 ka and ca. 15 ka are both <1.1 mm/yr (Figs. 6C and 6D). Along the Yunlong reach, the river incision rates are <2.8 mm/yr and <2.3 mm/yr for two higher strath terraces since 100 ka and 70 ka, respectively (Fig. 6E).

In summary, the rates of river incision since the late Pleistocene along the Lancang River have decelerated upstream (Figs. 6 and 7). Incision rates averaged over ~100 k.y. decrease from <2.8 mm/yr below the knickzone to <2.1 mm/yr at the knickzone. Incision rates averaged over the last ~45 k.y. decrease upstream from <2.3 mm/yr below the knickzone to <1.7 mm/yr at

the knickzone and to <0.5 mm/yr above the knickzone. In addition, incision rates at the knickzone appear to decrease temporally from <1.7–2.1 mm/yr since the late Pleistocene to <1.1 mm/yr since the Holocene.

DISCUSSION

Our work reveals the following spatiotemporal pattern of river incision along the Lancang River (Figs. 6 and 7): (1) river aggradation occurred at >120–100 ka, ca. 90–70 ka, ca. 25–15 ka, and <9 ka, followed by river incision starting at ca. 100 ka, ca. 45 ka, ca. 15 ka, and ca. 6 ka, respectively; (2) the incision rates since the late Pleistocene vary between <0.5 mm/yr and 2.8 mm/yr; (3) the incision rates since the late Pleistocene decrease upstream; and (4) the incision rates at the knickzone decreased from ca. 100 ka to ca. 10 ka. Next, we first evaluate the uncertainties in our terraced-derived river incision rates. This allows us to quantitatively compare our results against the regionally averaged erosion rates estimated by thermochronological dating and cosmogenic nuclide concentrations. Potential factors controlling the competing erosional processes at different temporal and spatial scales are discussed.

Uncertainties in the Estimated River Incision Rates

Systematic overestimation of river incision rates can occur if the dated terrace sediments were deposited significantly later than strath formation.

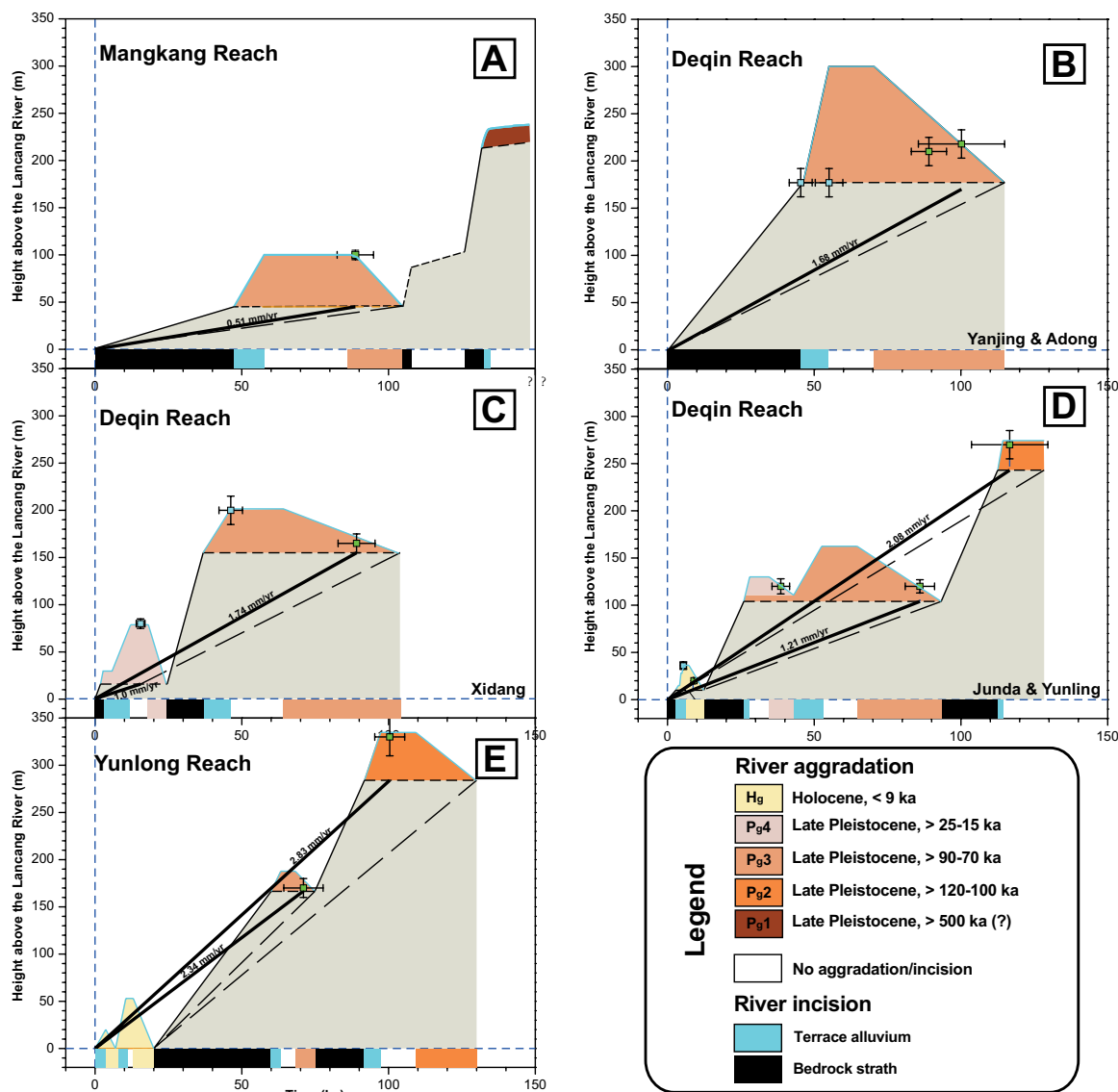


Figure 6. Plots of optically stimulated luminescence (OSL) and cosmogenic radionuclide (CRN) age results vs. height above the Lancang River for fluvial terraces along three reaches of the Lancang River, together with interpretation for the aggradation-incision history and river incision rates: (A) Mangkang reach; (B) Deqin reach at Yanjing; (C) Deqin reach at Xidang; (D) Deqin reach at Junda and Yunling; and (E) Yunlong reach. The symbol for the ages is a square with error bars: green for OSL and cyan for CRN.

Wide valleys tend to store thick sequences of alluvial sediments that protect the underlying bedrock strath from subsequent episodes of incision. In addition, poor exposure of terrace sediment sequences due to dense vegetation and farming activities may lead to preferred OSL dating of fine-grained overbank deposits, which could make the resulting age estimates younger than the timing of deposition of the first, coarser-grained sediments after beveling the bedrock strath. Potential overestimation of the strath height above the river may be introduced due to the uneven strath-alluvium contact, such as gently dipping bedrock straths in wide river channels. It is difficult to confidently exclude or quantify such uncertainties in the age estimates of strath formation and in the height estimates of the strath surfaces. Among the three river reaches that we investigated, the narrow Lancang River channel within the knickzone probably suffers less from these uncertainties compared to the wider Yunlong reach below the knickzone. Hence, a lower bound of strath height for the lower

terrace at Yunlong is estimated to be 130 ± 20 m, which was obtained by projecting the gently dipping bedrock strath to the present-day position of the Lancang River. Together with the older burial age of the higher terrace (100.4 ± 5.1 ka), this would yield a minimum incision rate of ~ 1.3 mm/yr below the knickzone, which decreases to more than one half of the uncorrected value of < 2.3 mm/yr and is slightly lower than that at the knickzone (Figs. 2 and 7).

Erosion Rates at Different Time Scales in Southeast Tibet

The incision rates calculated from fluvial terraces along the Lancang River in this study vary between 0.5 and 2.8 mm/yr since the late Pleistocene. The exact rate depends strongly on the ages of strath development as constrained by our dating of the overlying terrace deposits. Even in the presence of unquantified uncertainties, these values are significantly higher

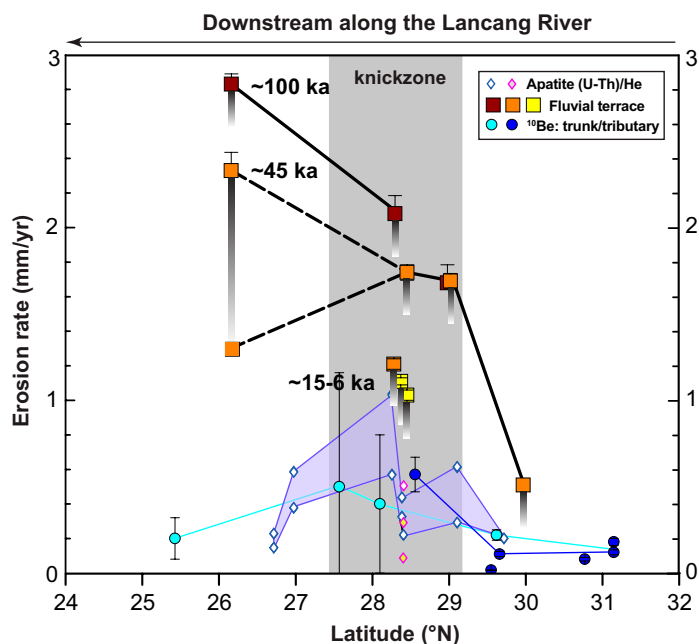


Figure 7. Comparison among erosion rates estimated by three techniques along the Lancang River, including apatite (U-Th)/He dating shown as blue diamonds filled with white color from Yang et al. (2016), and purple diamonds filled with white color for river valley samples and yellow color for ridge-top samples from Liu-Zeng et al. (2018), detrital ^{10}Be concentrations for both main trunks (intermediate reaches, circles filled with cyan color) and tributaries (circles filled with dark-blue color; Henck et al., 2011), and fluvial terraces in this study (squares). The upper bound value of river incision rate is marked by a square with a gray-gradient strip showing the uncertainty, which is mainly due to the time lag between strath formation and terrace sediment deposition.

than landscape-scale erosion rates estimated from low-temperature thermochronometry and cosmogenic ^{10}Be concentrations in river sediments (Fig. 7). Apatite (U-Th)/He dating of bedrock samples from ridge tops yields average erosion rates since the late Miocene of $\sim 0.1\text{--}0.3$ mm/yr (Liu-Zeng et al., 2018), whereas samples from near the valley bottom of the Lancang River yield erosion rates since the late Miocene of $\sim 0.4\text{--}1.0$ mm/yr (Yang et al., 2016). These rates are similar to millennial-scale catchment-averaged denudation rates of $\sim 0.2\text{--}0.6$ mm/yr, which are based on ^{10}Be concentrations in modern river sand sampled from either the main stem or from tributaries along the Lancang River (Henck et al., 2011).

The different erosion rates estimated using three different methods from samples collected at different locations may reflect erosion processes that operate at different temporal and spatial scales. For example, the response of hillslopes could lag behind a recently accelerated trunk river incision event. In this context, our faster river incision rates compared to the million-year time scale exhumation rates may indicate that the trunk of the Lancang River incised faster than the surrounding hillslopes. This interpretation is compatible with ^{10}Be -derived denudation rates of the Lancang River at 1–10 k.y. time scales that are lower than our trunk-river incision rates (Henck et al., 2011), because the former are spatially weighted values over the very large drainage area of the Lancang River, where the upland has relatively lower erosion rates than the valley bottom (Henck et al., 2011; McPhillips et al., 2016).

Another possible explanation for the difference between the long (>1 m.y.) and short (<100 k.y.) time scale erosion rates in southeast Tibet is the nonsteady process of river incision into bedrock, in that periods of

incision are punctuated by episodic incision hiatuses (e.g., Gardner et al., 1987; Mills, 2000; Finnegan et al., 2014). The terrace-derived incision rates in this study cover time scales of $10^4\text{--}10^5$ yr, whereas erosion rates from thermochronology are averaged over 10^6 yr. Finnegan et al. (2014) have shown that estimated fluvial incision rates will be larger, due to the shorter measurement interval, if hiatuses in river incision have a heavy-tailed length distribution (cf. Ganti et al., 2016). Our dating results suggest that episodes of river aggradation above bedrock strath surfaces persisted for $>10^4$ yr (Fig. 6), but we cannot judge whether hiatuses in river incision truly follow a heavy-tailed distribution. In any case, in contrast to what would be expected for a heavy-tailed distribution, we observe the opposite: a decrease in the incision rate with decreasing measurement interval. In other words, if the hiatus distribution were heavy-tailed, the actual increase in incision rate with decreasing time scale would be even greater.

Our observations also suggest that hiatuses in river incision into bedrock are not coupled in a simple way to periodic glacial-interglacial climatic cycles, as documented elsewhere (e.g., Gardner et al., 1987; Mills, 2000; Finnegan et al., 2014). Alternating transient pulses of river aggradation and incision have been documented at several locations along the margins of the Tibetan Plateau, with the transition occurring at ca. 140 ka, ca. 96–106 ka, 53–40 ka, 18.6–15.3 ka, ca. 9 ka, ca. 5.2 ka, and 3.6 ka (Harkins et al., 2007; Dey et al., 2016). These times are often coincident with those revealed in this study along the Lancang River in southeast Tibet and may point to regional causes such as shifts in monsoon strength, perhaps coupled to glacial cycles (e.g., Srivastava et al., 2008; Scherler et al., 2015).

Overall, it is striking that deeply entrenched bedrock rivers in southeast Tibet still preserve coherent strath terraces up to 150 m high above the modern river that are older than 90 ka. The terraces demonstrate that the Lancang River has experienced intermittent incision, i.e., phases of rapid incision, separated by long periods of quiescence or aggradation. Processes such as climatic shifts, landslides, or tectonic or glacial ponding (e.g., Kong et al., 2009; Wang et al., 2014; Scherler et al., 2014, 2016) can lead to long periods of aggradation that are followed by river lateral abrasion and formation of terraces, which are abandoned during subsequent periods of fast incision. We are inclined to believe that along the Lancang River, complex relationships among tectonic uplift, climate, and surface processes may control the nonsteady bedrock river incision (Burbank et al., 1996; Whipple, 2001; Whittaker et al., 2007; Finnegan et al., 2014; Gallen et al., 2015).

Spatiotemporal Variations in River Incision Rates

River aggradation along the Lancang River occurred at $>120\text{--}100$ ka, ca. 90–70 ka, ca. 25–15 ka, and <9 ka, each followed by incision periods that started at ca. 100 ka, ca. 45 ka, ca. 15 ka, and ca. 6 ka, respectively (Fig. 6). A notable feature in this history is that after 100 m of aggradation at 90–70 ka, there has been >150 m of incision since ca. 45 ka. The stalagmite oxygen-isotope records in southeast Tibet (Xiaobailong [XBL] Cave in Fig. 1A) reflect the variability in the Indian summer monsoon precipitation, which varies on orbital time scales (Fig. 8B; Cai et al., 2015). Furthermore, moraine ages in southeast Tibet are clustered at 105 ± 10 ka, 50 ± 10 ka, and 15 ± 5 ka, indicating that glaciers advanced during marine isotope stages (MIS) 5C, 3, and 2/1 (Fu et al., 2013, and reference therein), at times when the climate was cold but also wet enough (Fig. 8C). Periods of river incision from this study occurred both during cold, glacial periods as well as during warmer and wetter interglacial periods (e.g., Bridgland and Westaway, 2008). It is worth noting, however, that our reconstructed periods of river aggradation and incision may be incomplete due to limited dating opportunities along the Lancang River. In

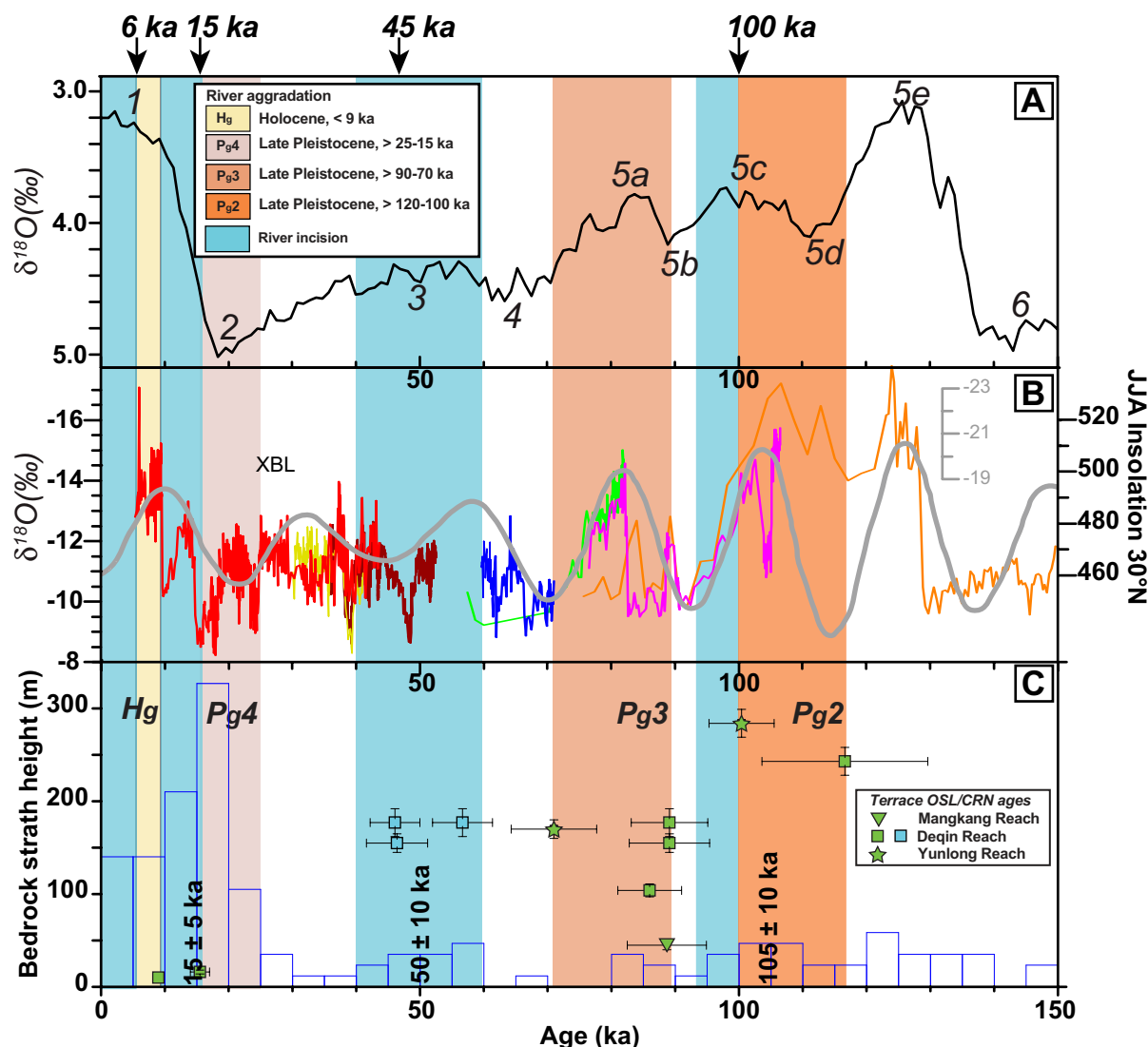


Figure 8. (A) Isotopic composition of the oceans viewed at the time scale of 0–150 k.y., modified after Lisiecki and Raymo (2005). Labels next to peaks and troughs refer to isotopic stages. Stage 5e, for example, represents the last interglacial period. (B) Terrestrial cave speleothem $\delta^{18}\text{O}$ values from Xiaobailong Cave (XBL) in southeast Tibet (Cai et al., 2015). Gray line shows the summer insolation at 30°N integrated over June, July, and August (JJA) as calculated by Berger and Loutre (1991) for the last 10 m.y. (C) Plot of optically stimulated luminescence (OSL) and cosmogenic radionuclide (CRN) ages vs. bedrock strath heights for fluvial terraces in this study, and histogram of glacial deposit ages in southeast Tibet (Fu et al., 2013, and reference therein). See Figure 2 for deposit abbreviations.

summary, it is presently difficult to assign clear cause-and-effect relationships to periods of river aggradation and incision in southeast Tibet, but there appears to be a tendency for prolonged periods of aggradation during glacial periods, punctuated by periods of incision, when strong monsoon precipitation increases river discharge (e.g., Scherler et al., 2015). The actual timing of individual aggradation and incision periods may result from the complex hydrologic response to climate changes and other factors that influence sediment storage and transport (e.g., Pederson et al., 2006; Pazzaglia, 2013).

Our work resolves the spatial pattern of river incision along the Lancang River since the late Pleistocene. The spatial pattern for the Holocene incision is not resolved, however. River incision rates since the late Pleistocene decrease between 26°N and 30°N, from <2.3 mm/yr below the knickzone, to <1.7 mm/yr at the knickzone, and to <0.5 mm/yr above

the knickzone (Fig. 7). This pattern of upstream-decreasing incision rates is different from that of other proxies of erosion at either shorter or longer time scales. However, the river incision rate at the knickzone since the Holocene is <1.1 mm/yr, which is similar to other proxies of erosion. Other proxies of erosion include river steepness, detrital ^{10}Be concentrations, and low-temperature thermochronological data, and all yield the maximum values within the knickzone (Fig. 7). Normalized channel steepness indices indicate greater erosional efficiency at the knickzone that drop markedly below and above the knickzone (Fig. 1C). This pattern is corroborated by ^{10}Be -derived denudation rates from either the main stem of the Lancang River or its tributaries (Henck et al., 2011), as well as apatite (U-Th)/He dating of bedrock samples across the knickzone (Fig. 7; Yang et al., 2016; Liu-Zeng et al., 2018). The spatial and temporal pattern of river incision rates along the Lancang River indicates that river

incision rates since the late Pleistocene are decoupled from other proxies of erosion. Moreover, the late Pleistocene river incision rates below the knickzone are similar to or even higher than that within the knickzone.

Together with the fact that river incision initiated during the cold, glacial periods, this pattern suggests that surface processes related to the Pleistocene glacial cycles could have controlled not only the timing of river incision but also the spatiotemporal pattern. At present, monsoonal moisture along the Lancang valley decreases dramatically upstream, and it drops down to 20% at the transition with the high plateau area near Deqin (Fig. 1C). This pattern may imply higher water discharge below the knickzone. During glacial periods, additional snowmelt runoff may have occurred along all the reaches, especially downstream of high massifs, where higher topography experienced lower temperatures and greater proximity to the peak led to greater total precipitation (Bookhagen and Burbank, 2010), such as the Yunlong reach, which is primarily located below the knickzone. Because strengthened precipitation tends to facilitate slope failures by increasing pore pressures in hillslopes (e.g., Pratt et al., 2002), the increase in sediment supply is often invoked in terms of high frequency of landslide activity. Furthermore, because the Lancang valley is very narrow at the Yanjing-Weixi knickzone, and it is surrounded by high and glaciated mountains, it appears to be prone to ephemeral damming by glaciers and/or landslides, as observed in other places along the margin of the Tibetan Plateau (Montgomery et al., 2004; Ouimet et al., 2007; Lang et al., 2013; Scherler et al., 2014). When such natural dams fail, they can trigger catastrophic outburst floods that have the potential to account for very high incision rates in the valley below the knickzone. In addition to climatic factors, tectonics may also play a role in modulating the behavior of fluvial systems in tectonically active regions, by creating differential uplift, local steepening of the river profile, and rapid river incision (e.g., Merritts et al., 1994; Hetzel et al., 2006; Wegmann and Pazzaglia, 2009), or tilting blocks, regional flattening of the river profile, and river aggradation (e.g., Humphrey and Konrad, 2000; Wang et al., 2014). Further work is needed to evaluate how local to regional tectonic events have contributed to the spatiotemporal pattern of river incision rates along the Lancang River in southeast Tibet.

CONCLUSION

This study reports for the first time remarkably well-preserved fluvial terraces along three reaches of the Lancang River in the high-relief region of southeast Tibet. Episodic river aggradation occurred at >120–100 ka, 90–70 ka, 25–15 ka, and <9 ka, followed by periods of incision that initiated at ca. 100 ka, ca. 45 ka, ca. 15 ka, and ca. 6 ka, respectively. This timing indicates that alternating periods of aggradation and incision were controlled by orbital-driven changes in monsoon strength. Rates of river incision since the late Pleistocene have varied between <0.5 and 2.8 mm/yr, and they are more than an order of magnitude higher than million-year time scale erosion rates derived from bedrock thermochronologic data and thousand-year time scale denudation rates from cosmogenic ¹⁰Be concentrations in modern river sand. This difference and the spatiotemporal patterns of incision suggest that erosion is not constant, either in space or time, and it is sensitive to measurement time scales and dominant surface processes. Notably, we observed that the river incision rate since the late Pleistocene below the knickzone is higher than that at the knickzone, and this is in contrast to the spatial pattern of other erosion proxies, which show a maximum value at the knickzone. In addition, the rates of river incision since the Holocene at the knickzone decrease through time. Our results thus demonstrate that climatic changes in the big drainage system of the Lancang River modulate the spatial and temporal pattern of river incision in southeast Tibet.

ACKNOWLEDGMENTS

Detailed and constructive comments by two anonymous reviewers greatly helped to improve the data description and final interpretations of this work. We gratefully acknowledge the joint support by the National Key Research and Development Project of China (2016YFC0600310), the National Natural Science Foundation of China (41502188, 4176114406, 41225010), and China Earthquake Administration (IGCEA1421). We thank Ning Zhong for assistance in the field, Chang-Sheng Wang for help with optically stimulated luminescence dating, Rong-Zhang Zheng for help with mineral separation, and Luca Malatesta and Hui-Ping Zhang for helpful discussion.

REFERENCES CITED

- Aitken, M.J., 1998, *An Introduction to Optical Dating*: Oxford, UK, Oxford University Press, 267 p.
- Anderson, R.S., Repka, J.L., and Dick, G.S., 1996, Explicit treatment of inheritance in dating depositional surfaces using in situ ¹⁰Be and ²⁶Al: *Geology*, v. 24, no. 1, p. 47–51, [https://doi.org/10.1130/0091-7613\(1996\)024<0047:ETOID>2.3.CO;2](https://doi.org/10.1130/0091-7613(1996)024<0047:ETOID>2.3.CO;2).
- Balco, G., Stone, J.O., Lifton, N.A., and Dunai, T.J., 2008, A complete and easily accessible means of calculating surface exposure ages or erosion rates from ¹⁰Be and ²⁶Al measurements: *Quaternary Geochronology*, v. 3, no. 3, p. 174–195, <https://doi.org/10.1016/j.quageo.2007.12.001>.
- Berger, A., and Loutre, M.F., 1991, Insolation values for the climate of the last 10 million years: *Quaternary Science Reviews*, v. 10, p. 297–317, [https://doi.org/10.1016/0277-3791\(91\)90033-O](https://doi.org/10.1016/0277-3791(91)90033-O).
- Bookhagen, B., and Burbank, D.W., 2010, Toward a complete Himalayan hydrological budget: Spatiotemporal distribution of snowmelt and rainfall and their impact on river discharge: *Journal of Geophysical Research*, v. 115, F03019, <https://doi.org/10.1029/2009JF001426>.
- Bridgland, D., and Westaway, R., 2008, Climatically controlled river terrace staircases: A worldwide Quaternary phenomenon: *Geomorphology*, v. 98, no. 3, p. 285–315, <https://doi.org/10.1016/j.geomorph.2006.12.032>.
- Brookfield, M.E., 1998, The evolution of the great river systems of southern Asia during the Cenozoic India-Asia collision: Rivers draining southwards: *Geomorphology*, v. 22, no. 3–4, p. 285–312, [https://doi.org/10.1016/S0169-555X\(97\)00082-2](https://doi.org/10.1016/S0169-555X(97)00082-2).
- Burbank, D.W., Leland, J., Fielding, E., Anderson, R.S., Brozovic, N., Reid, M.R., and Duncan, C., 1996, Bedrock incision, rock uplift and threshold hillslopes in the northwestern Himalayas: *Nature*, v. 379, p. 505–510, <https://doi.org/10.1038/10338/379505a0>.
- Burchfiel, B.C., and Chen, Z.L., 2012, Tectonics of the Southeastern Tibetan Plateau and its Adjacent Foreland: *Geological Society of America Memoir* 210, 231 p., <https://doi.org/10.1130/2012.1210>.
- Cai, Y.J., Fung, I.Y., Edwards, R.L., An, Z.S., Cheng, H., Lee, J.E., Tan, L.C., Shen, C.C., Wang, X.F., Day, J.A., Zhou, W.J., Kelly, M.J., and Chiang, J., 2015, Variability of stalagmite-inferred Indian monsoon precipitation over the past 252,000 y: *Proceedings of the National Academy of Sciences of the United States of America*, v. 112, no. 10, p. 2954–2959, <https://doi.org/10.1073/pnas.1424035112>.
- Clark, M.K., Schoenbohm, L.M., Royden, L.H., Whipple, K.X., Burchfiel, B.C., Zhang, X., Tang, W., Wang, E., and Chen, L., 2004, Surface uplift, tectonics, and erosion of eastern Tibet from large-scale drainage patterns: *Tectonics*, v. 23, TC1006, <https://doi.org/10.1029/2002TC001402>.
- Clark, M.K., House, M.A., Royden, L.H., Whipple, K.X., Burchfiel, B.C., Zhang, X., and Tang, W., 2005, Late Cenozoic uplift of southeastern Tibet: *Geology*, v. 33, p. 525–528, <https://doi.org/10.1130/G21265.1>.
- Clark, M.K., Royden, L.H., Whipple, K.X., Burchfiel, B.C., Zhang, X., and Tang, W., 2006, Use of a regional, relict landscape to measure vertical deformation of the eastern Tibetan Plateau: *Journal of Geophysical Research*, v. 111, F03002, <https://doi.org/10.1029/2005JF000294>.
- Deng, Q.D., Zhang, P.Z., Ran, Y.K., Yang, X., Min, W., and Chu, Q.Z., 2003, Basic characteristics of active tectonics of China: *Science in China Series D: Earth Science*, v. 46, no. 3, p. 356–372.
- Dewald, A., Heinze, S., Jolie, J., Zilges, A., Dunai, T., Rethemeyer, J., Melles, M., Staubwasser, M., Kuczewski, B., Richter, J., Radtke, U., von Blankenburg, F., and Klein, M., 2013, CologneAMS, a dedicated center for accelerator mass spectrometry in Germany: *Nuclear Instruments & Methods in Physics Research, Section B, Beam Interactions with Materials and Atoms*, v. 294, p. 18–23, <https://doi.org/10.1016/j.nimb.2012.04.030>.
- Dey, S., Thiede, R.C., Schildgen, T.F., Wittmann, Bookhagen, B., Scherler, D., Jain, V., and Strecker, M.R., 2016, Climate-driven sediment aggradation and incision since the late Pleistocene in the NW Himalaya, India: *Earth and Planetary Science Letters*, v. 449, p. 321–331, <https://doi.org/10.1016/j.epsl.2016.05.050>.
- Dunai, T.J., 2010, *Cosmogenic Nuclides: Principles, Concepts and Applications in the Earth Surface Sciences*: Cambridge, UK, Cambridge University Press, 198 p., <https://doi.org/10.1017/CBO9780511804519>.
- Dunne, J., Elmore, D., and Muzikar, P., 1999, Scaling factors for the rates of production of cosmogenic nuclides for geometric shielding and attenuation at depth on sloped surfaces: *Geomorphology*, v. 27, no. 1, p. 3–11, [https://doi.org/10.1016/S0169-555X\(98\)00086-5](https://doi.org/10.1016/S0169-555X(98)00086-5).
- Finnegan, N.J., and Dietrich, W.E., 2011, Episodic bedrock strath terrace formation due to meander migration and cutoff: *Geology*, v. 39, no. 2, p. 143–146, <https://doi.org/10.1130/G31716.1>.
- Finnegan, N.J., Schumer, R., and Finnegan, S., 2014, A signature of transience in bedrock river incision rates over timescales of 10⁴–10⁷ years: *Nature*, v. 505, p. 391–394, <https://doi.org/10.1038/nature12913>.
- Fu, P., Stroeve, A.P., Harbor, J.M., Hättestrand, Heyman, J., Caffè, M.W., and Zhou, L.P., 2013, Paleoglaciation of Shaluli Shan, southeastern Tibetan Plateau: *Quaternary Science Reviews*, v. 64, p. 121–135, <https://doi.org/10.1016/j.quascirev.2012.12.009>.
- Gallen, S.F., Pazzaglia, F.J., Wegmann, K.W., Pederson, J.L., and Gardner, T.W., 2015, The dynamic reference frame of rivers and apparent transience in incision rates: *Geology*, v. 43, no. 7, p. 623–626, <https://doi.org/10.1130/G36692.1>.
- Ganti, V., von Hagke, C., Scherler, D., Lamb, M.P., Fischer, W.W., and Avouac, J.P., 2016, Time scale bias in erosion rates of glaciated landscapes: *Science Advances*, v. 2, no. 10, p. e1600204, <https://doi.org/10.1126/sciadv.1600204>.

- Gardner, T.W., Jorgensen, D.W., Shuman, C., and Lemieux, C.R., 1987, Geomorphic and tectonic process rates: Effects of measured time interval: *Geology*, v. 15, p. 259–261, [https://doi.org/10.1130/0091-7613\(1987\)15<259:GATPRE>2.0.CO;2](https://doi.org/10.1130/0091-7613(1987)15<259:GATPRE>2.0.CO;2).
- Gosse, J.C., and Phillips, F.M., 2001, Terrestrial in situ cosmogenic nuclides: Theory and application: *Quaternary Science Reviews*, v. 20, no. 14, p. 1475–1560, [https://doi.org/10.1016/S0277-3791\(00\)00171-2](https://doi.org/10.1016/S0277-3791(00)00171-2).
- Gregory, J.W., and Gregory, C.J., 1925, The geology and physical geography of Chinese Tibet, and its relations to the mountain system of south-eastern Asia, from observations made during the Percy Sladen Expedition 1922: *Philosophical Transactions of the Royal Society of London, Series B, Biological Sciences*, v. 213, p. 171–298, <https://doi.org/10.1098/rstb.1925.0005>.
- Hallet, B., and Molnar, P., 2001, Distorted drainage basins as markers of crustal strain east of the Himalaya: *Journal of Geophysical Research*, v. 106, p. 13,697–13,709, <https://doi.org/10.1029/2000JB900335>.
- Hancock, G.S., and Anderson, R.S., 2002, Numerical modeling of fluvial strath-terrace formation in response to oscillating climate: *Geological Society of America Bulletin*, v. 114, p. 1131–1142.
- Harkins, N., Kirby, E., Heimsath, A., Robinson, R., and Reiser, U., 2007, Transient fluvial incision in the headwaters of the Yellow River, northeastern Tibet, China: *Journal of Geophysical Research*, v. 112, F03S04, <https://doi.org/10.1029/2006JF000570>.
- Henck, A.C., Montgomery, D.R., Huntington, K.W., and Liang, C., 2010, Monsoon control of effective discharge, Yunnan and Tibet: *Geology*, v. 38, no. 11, p. 975–978, <https://doi.org/10.1130/G31444.1>.
- Henck, A.C., Huntington, K.W., Stone, J.O., Montgomery, D.R., and Hallet, B., 2011, Spatial controls on erosion in the Three Rivers region, southeastern Tibet and southwestern China: *Earth and Planetary Science Letters*, v. 303, no. 1, p. 71–83, <https://doi.org/10.1016/j.epsl.2010.12.038>.
- Hetzl, R., Niedermann, S., Tao, M.X., Kubik, P.W., and Strecker, M.R., 2006, Climatic versus tectonic control on river incision at the margin of NE Tibet: ¹⁰Be exposure dating of river terraces at the mountain front of the Qilian Shan: *Journal of Geophysical Research*, v. 111, F03012, <https://doi.org/10.1029/2005JF000352>.
- Humphrey, N.F., and Konrad, S.K., 2000, River incision or diversion in response to bedrock uplift: *Geology*, v. 28, no. 1, p. 43–46, [https://doi.org/10.1130/0091-7613\(2000\)28<43:RIODIR>2.0.CO;2](https://doi.org/10.1130/0091-7613(2000)28<43:RIODIR>2.0.CO;2).
- Kong, P., Na, C.G., Fink, D., Zhao, X.T., and Xiao, W., 2009, Moraine dam related to late Quaternary glaciation in the Yulong Mountains, southwest China, and impacts on the Jinsha River: *Quaternary Science Reviews*, v. 28, no. 27, p. 3224–3235, <https://doi.org/10.1016/j.quascirev.2009.08.005>.
- Lal, D., 1991, Cosmic-ray labeling of erosion surfaces: In situ nuclide production rates and erosion models: *Earth and Planetary Science Letters*, v. 104, no. 2–4, p. 424–439, [https://doi.org/10.1016/0012-821X\(91\)90220-C](https://doi.org/10.1016/0012-821X(91)90220-C).
- Lambeck, K., Antonioli, F., Purcell, A., and Silenzi, S., 2004, Sea level change along the Italian coast for the past 10,000 yr: *Quaternary Science Reviews*, v. 23, no. 14–15, p. 1567–1598, <https://doi.org/10.1016/j.quascirev.2004.02.009>.
- Lang, K.A., Huntington, K.W., and Montgomery, D.R., 2013, Erosion of the Tsongpo Gorge by megafloods, Eastern Himalaya: *Geology*, v. 41, p. 1003–1006, <https://doi.org/10.1130/G34693.1>.
- Lavé, J., and Avouac, J.P., 2001, Fluvial incision and tectonic uplift across the Himalayas of central Nepal: *Journal of Geophysical Research*, v. 106, p. 26,561–26,591.
- Lisiecki, L.E., and Raymo, M.E., 2005, A Pliocene–Pleistocene stack of 57 globally distributed benthic $\delta^{18}\text{O}$ records: *Paleoceanography*, v. 20, no. 1, PA1003, <https://doi.org/10.1029/2004PA001071>.
- Liu-Zeng, J., Tapponnier, P., Gaudemer, Y., and Ding, L., 2008, Quantifying landscape differences across the Tibetan Plateau: Implications for topographic relief evolution: *Journal of Geophysical Research*, v. 113, F04018, <https://doi.org/10.1029/2007JF000897>.
- Liu-Zeng, J., Zhang, J.Y., McPhillips, D., Reiners, P., Wang, W., Pik, R., Zeng, L.S., Hoke, G., Xie, K.J., Xiao, P., Zheng, D.W., and Ge, Y.K., 2018, Multiple episodes of fast exhumation since the Late Cretaceous in southeast Tibet, revealed by low-temperature thermochronology: *Earth and Planetary Science Letters*, v. 490, p. 62–76, <https://doi.org/10.1016/j.epsl.2018.03.011>.
- Lu, Y.C., Wang, X.L., and Wintle, A.G., 2007, A new OSL chronology for dust accumulation in the last 130,000 yr for the Chinese Loess Plateau: *Quaternary Research*, v. 67, no. 1, p. 152–160, <https://doi.org/10.1016/j.yqres.2006.08.003>.
- McPhillips, D., Hoke, G.D., Liu-Zeng, J., Bierman, P.R., Rood, D.H., and Niedermann, S., 2016, Dating the incision of the Yangtze River Gorge at the First Bend using three-nuclide burial ages: *Geophysical Research Letters*, v. 43, p. 101–110, <https://doi.org/10.1002/2015GL066780>.
- Merritts, D.J., Vincent, K.R., and Wohl, E.E., 1994, Long river profiles, tectonism, and eustasy: A guide to interpreting fluvial terraces: *Journal of Geophysical Research*, v. 99, p. 14,031–14,050, <https://doi.org/10.1029/94JB00857>.
- Mills, H.H., 2000, Apparent increasing rates of stream incision in the eastern United States during the late Cenozoic: *Geology*, v. 28, p. 955–957, [https://doi.org/10.1130/0091-7613\(2000\)28<955:AIROSI>2.0.CO;2](https://doi.org/10.1130/0091-7613(2000)28<955:AIROSI>2.0.CO;2).
- Montgomery, D.R., Hallet, B., Liu, Y.P., Finnegan, N., Anders, A., Gillespie, A., and Greenberg, H.M., 2004, Evidence for Holocene megafloods down the Tsongpo River gorge, southeastern Tibet: *Quaternary Research*, v. 62, p. 201–207, <https://doi.org/10.1016/j.yqres.2004.06.008>.
- Mudd, S.M., Attal, M., Milodowski, D.T., Grieve, S.W.D., and Valters, D.A., 2014, A statistical framework to quantify spatial variation in channel gradients using the integral method of channel profile analysis: *Journal of Geophysical Research*, v. 119, no. 2, p. 138–152, <https://doi.org/10.1002/2013JF00298>.
- Murray, A.S., and Wintle, A.G., 2003, The single aliquot regenerative dose protocol: Potential for improvements in reliability: *Radiation Measurements*, v. 37, no. 4, p. 377–381, [https://doi.org/10.1016/S1350-4487\(03\)00053-2](https://doi.org/10.1016/S1350-4487(03)00053-2).
- Quimet, W.B., Whipple, K.X., Royden, L.H., Sun, Z.M., and Chen, Z.L., 2007, The influence of large landslides on river incision in a transient landscape: Eastern margin of the Tibetan Plateau (Sichuan, China): *Geological Society of America Bulletin*, v. 119, no. 11–12, p. 1462–1476, <https://doi.org/10.1130/B26136.1>.
- Quimet, W., Whipple, K., Royden, L., Reiners, P., Hodges, K., and Pringle, M., 2010, Regional incision of the eastern margin of the Tibetan Plateau: *Lithosphere*, v. 2, no. 1, p. 50–63, <https://doi.org/10.1130/L57.1>.
- Pan, G.T., Ding, J., Yao, D.S., and Wang, L.Q., 2004, Geological Map of Qinghai-Xiang (Tibet) Plateau and Adjacent Areas: Chengdu, China, Chengdu Institute of Geology and Mineral Resources, China Geological Survey, scale 1:1,500,000, 6 sheets.
- Pazzaglia, F.J., 2013, Fluvial terraces, in Wohl, E., ed., *Treatise on Geomorphology Volume 9: Treatise on Fluvial Geomorphology*: San Diego, California, Academic Press, p. 379–412, <https://doi.org/10.1016/B978-0-12-374739-6.00248-7>.
- Pederson, J.L., Anders, M.D., Rittenhour, T.M., Sharp, W.D., Gosse, J.C., and Karlstrom, K.E., 2006, Using fill terraces to understand incision rates and evolution of the Colorado River in eastern Grand Canyon, Arizona: *Journal of Geophysical Research*, v. 111, F02003, <https://doi.org/10.1029/2004JF000201>.
- Perron, J.T., and Royden, L., 2013, An integral approach to bedrock river profile analysis: *Earth Surface Processes and Landforms*, v. 38, no. 6, p. 570–576, <https://doi.org/10.1002/esp.3302>.
- Pratt, B., Burbank, D.W., Heimsath, A., and Ojha, T., 2002, Impulsive alluviation during early Holocene strengthened monsoons, central Nepal Himalaya: *Geology*, v. 30, p. 911–914, [https://doi.org/10.1130/0091-7613\(2002\)030<0911:IADEHS>2.0.CO;2](https://doi.org/10.1130/0091-7613(2002)030<0911:IADEHS>2.0.CO;2).
- Repka, J.L., Anderson, R.S., and Finkel, R.C., 1997, Cosmogenic dating of fluvial terraces, Fremont River, Utah: *Earth and Planetary Science Letters*, v. 152, no. 1, p. 59–73, [https://doi.org/10.1016/S0012-821X\(97\)00149-0](https://doi.org/10.1016/S0012-821X(97)00149-0).
- Rhodes, E.J., 2011, Optically stimulated luminescence dating of sediments over the past 200,000 years: *Annual Review of Earth and Planetary Sciences*, v. 39, p. 461–488, <https://doi.org/10.1146/annurev-earth-040610-133425>.
- Rodnight, H., Duller, G.A., Wintle, A.G., and Tooth, S., 2006, Assessing the reproducibility and accuracy of optical dating of fluvial deposits: *Quaternary Geochronology*, v. 1, no. 2, p. 109–120, <https://doi.org/10.1016/j.quageo.2006.05.017>.
- Scherler, D., Munack, H., Mey, J., Eugster, P., Wittmann, H., Codilean, A.T., and Strecker, M.R., 2014, Ice dams, outburst floods, and glacial incision at the western margin of the Tibetan Plateau: A >100 k.y. chronology from the Shyok Valley, Karakoram: *Geological Society of America Bulletin*, v. 126, no. 5–6, p. 738–758, <https://doi.org/10.1130/B30942.1>.
- Scherler, D., Bookhagen, B., Wulf, H., Preusser, F., and Strecker, M.R., 2015, Increased late Pleistocene erosion rates during fluvial aggradation in the Garhwal Himalaya, northern India: *Earth and Planetary Science Letters*, v. 428, p. 255–266, <https://doi.org/10.1016/j.epsl.2015.06.034>.
- Scherler, D., Lamb, M.P., Rhodes, E.J., and Avouac, J.P., 2016, Climate-change versus landslide origin of fill terraces in a rapidly eroding bedrock landscape: San Gabriel River, California: *Geological Society of America Bulletin*, v. 128, no. 7–8, p. 1228–1248, <https://doi.org/10.1130/B31356.1>.
- Schoenbohm, L.M., Burchfiel, B.C., and Chen, L.Z., 2006, Propagation of surface uplift, lower crustal flow, and Cenozoic tectonics of the southeast margin of the Tibetan Plateau: *Geology*, v. 34, no. 10, p. 813–816, <https://doi.org/10.1130/G22679.1>.
- Srivastava, P., Tripathi, J.K., Islam, R., and Jaiswal, M.K., 2008, Fashion and phases of late Pleistocene aggradation and incision in the Alaknanda River valley, western Himalaya, India: *Quaternary Research*, v. 70, p. 68–80, <https://doi.org/10.1016/j.yqres.2008.03.009>.
- Stone, J.O., 2000, Air pressure and cosmogenic isotope production: *Journal of Geophysical Research*, v. 105, p. 23,753–23,759, <https://doi.org/10.1029/2000JB900181>.
- Tapponnier, P., Xu, Z.Q., Roger, F., Meyer, B., Arnaud, N., Wittlinger, G., and Yang, J.S., 2001, Oblique stepwise rise and growth of the Tibet Plateau: *Science*, v. 294, p. 1671–1677, <https://doi.org/10.1126/science.105978>.
- Taylor, M., and Yin, A., 2009, Active structures of the Himalayan-Tibetan orogen and their relationships to earthquake distribution, contemporary strain field, and Cenozoic volcanism: *Geosphere*, v. 5, no. 3, p. 199–214, <https://doi.org/10.1130/GES00217.1>.
- Thrasher, I.M., Mauz, B., Chiverrell, R.C., Lang, A., and Thomas, G., 2009, Testing an approach to OSL dating of late Devensian glaciofluvial sediments of the British Isles: *Journal of Quaternary Science*, v. 24, no. 7, p. 785–801, <https://doi.org/10.1002/jqs.1253>.
- Tian, Y.T., Kohn, B.P., Gleadow, A.J.W., and Hu, S.B., 2014, A thermochronological perspective on the morphotectonic evolution of the southeastern Tibetan Plateau: *Journal of Geophysical Research*, v. 119, p. 676–698, <https://doi.org/10.1002/2013JB010429>.
- von Blanckenburg, F., and Willenbring, J.K., 2014, Cosmogenic nuclides: Dates and rates of Earth-surface change: *Elements*, v. 10, no. 5, p. 341–346, <https://doi.org/10.2113/gselements.10.5.341>.
- von Blanckenburg, F., Hewawasam, T., and Kubik, P.W., 2004, Cosmogenic nuclide evidence for low weathering and denudation in the wet, tropical highlands of Sri Lanka: *Journal of Geophysical Research*, v. 109, F03008, <https://doi.org/10.1029/2003JF000049>.
- Wang, P., Scherler, D., Liu-Zeng, J., Mey, J., Avouac, J.P., Zhang, Y.D., and Shi, D.G., 2014, Tectonic control of Yarlung Tsangpo Gorge revealed by a buried canyon in southern Tibet: *Science*, v. 346, no. 6212, p. 978–981, <https://doi.org/10.1126/science.1259041>.
- Wang, X.L., Lu, Y.C., and Li, X.N., 2005, Luminescence dating of fine-grained quartz in Chinese loess—Simplified multiple aliquot regenerative-dose (MAR) protocol: *Dizhen Dizhi*, v. 27, p. 615–622.
- Wegmann, K.W., and Pazzaglia, F.J., 2009, Late Quaternary fluvial terraces of the Romagna and Marche Apennines, Italy: Climatic, lithologic, and tectonic controls on terrace genesis in an active orogeny: *Quaternary Science Reviews*, v. 28, no. 1, p. 137–165, <https://doi.org/10.1016/j.quascirev.2008.10.006>.
- Whipple, K.X., 2001, Fluvial landscape response time: How plausible is steady-state denudation?: *American Journal of Science*, v. 301, no. 4–5, p. 313–325, <https://doi.org/10.2475/ajs.3014-5.313>.

- Whipple, K.X., 2004, Bedrock rivers and the geomorphology of active orogens: Annual Review of Earth and Planetary Sciences, v. 32, p. 151–185, <https://doi.org/10.1146/annurev.earth.32.101802.120356>.
- Whittaker, A.C., 2012, How do landscapes record tectonics and climate?: Lithosphere, v. 4, no. 2, p. 160–164, <https://doi.org/10.1130/RFL003.1>.
- Whittaker, A.C., Cowie, P.A., Attal, M., Tucker, G.E., and Roberts, G.P., 2007, Bedrock channel adjustment to tectonic forcing: Implications for predicting river incision rates: Geology, v. 35, no. 2, p. 103–106, <https://doi.org/10.1130/G23106A.1>.
- Yang, R., Willett, S.D., and Goren, L., 2015, In situ low-relief landscape formation as a result of river network disruption: Nature, v. 520, p. 526–529, <https://doi.org/10.1038/nature14354>.
- Yang, R., Fellin, M.G., Herman, F., Willett, S.D., Wang, W., and Maden, C., 2016, Spatial and temporal pattern of erosion in the Three Rivers region, southeastern Tibet: Earth and Planetary Science Letters, v. 433, p. 10–20, <https://doi.org/10.1016/j.epsl.2015.10.032>.
- Zhang, H.P., Oskin, M.E., Liu-Zeng, J., Zhang, P.Z., Reiners, P.W., and Xiao, P., 2016, Pulsed exhumation of interior eastern Tibet: Implications for relief generation mechanisms and the origin of high-elevation planation surfaces: Earth and Planetary Science Letters, v. 449, p. 176–185, <https://doi.org/10.1016/j.epsl.2016.05.048>.
- Zhang, J.Y., Yin, A., Liu, W.C., Ding, L., and Xu, X.M., 2016, First geomorphological and sedimentological evidence for the combined tectonic and climate control on Quaternary Yarlung River diversion in the eastern Himalaya: Lithosphere, v. 8, no. 3, p. 293–316, <https://doi.org/10.1130/L500.1>.
- Zhang, Y.Z., Replumaz, A., Wang, G.C., Leloup, P.H., Gautheron, C., Bernet, M., van der Beek, P., Paquette, J.L., Wang, A., Zhang, K.X., Chevalier, M.L., and Li, H.B., 2015, Timing and rate of exhumation along the Litang fault system: Implication for fault reorganization in southeast Tibet: Tectonics, v. 34, p. 1219–1243, <https://doi.org/10.1002/2014TC003671>.

MANUSCRIPT RECEIVED 29 JUNE 2017
 REVISED MANUSCRIPT RECEIVED 21 JUNE 2018
 MANUSCRIPT ACCEPTED 2 AUGUST 2018

Erratum

ERRATUM: Spatiotemporal variation of late Quaternary river incision rates in southeast Tibet, constrained by dating fluvial terraces
 Jin-Yu Zhang, Jing Liu-Zeng, Dirk Scherler, An Yin, Wei Wang, Mao-Yun Tang, and Zhan-Fei Li

ORIGINAL ARTICLE: <https://doi.org/10.1130/L686.1>

ERRATUM PUBLICATION: <https://doi.org/10.1130/L686E.1>

When this article was originally published, several references to parts of Figure 2 were incorrect or inadvertently omitted on page 668. The corrections follow:

Page 668, left column, line 3 should read: (Table 1A; Figs. 2B, 2C, 4C, and 4E)

Page 668, left column, line 5 should read: (Table 1B; Figs. 2B, 2C, 4D, and 4E)

Page 668, left column, line 12 should read: (Table 1A; Figs. 2E, 4F, and 4G)

Page 668, left column, line 16 should read: (Table 1A; Figs. 2E and 4F)

Page 668, left column, line 22 should read: (Table 1; Figs. 2C and 4E)

Page 668, right column, line 5 should read: (Table 1; Figs. 2D, 4H, and 4I)

Page 668, right column, line 20 should read: Figs. 2F, 5B, and 5D